

Article

Characteristics of Vein-Forming Fluids in the Sinian Dengying Formation Reservoir and Its Relationship with the Hydrocarbon Accumulation Process in the Southwest and Southeast of the Sichuan Basin

Jing Luo ¹, Furong Wang ¹, Sheng He ^{1,*}, Zhiliang He ^{2,*}, Yahao Huang ³, Dianwei Zhang ⁴, Yanxian Zhu ¹, Ziming Sun ⁴ and Tao Luo ¹

¹ Key Laboratory of Tectonics and Petroleum Resources of Ministry of Education, China University of Geosciences (Wuhan), Wuhan 430074, China; luojing@cug.edu.cn (J.L.); wfr777@163.com (F.W.); 20131002224@cug.edu.cn (Y.Z.); cugluotao@cug.edu.cn (T.L.)

² Department of Science and Technology, China Petroleum & Chemical Corporation, Beijing 100728, China

³ Hubei Key Laboratory of Petroleum Geochemistry and Environment, Yangtze University, Wuhan 430100, China; hyhtr08916@cug.edu.cn

⁴ SINOPEC Petroleum Exploration and Production Research Institute, Beijing 100083, China; zhangdw.syky@sinopec.com (D.Z.); sunzm.syky@sinopec.com (Z.S.)

* Correspondence: shenghe@cug.edu.cn (S.H.); hezhiliang@sinopec.com (Z.H.)



Citation: Luo, J.; Wang, F.; He, S.; He, Z.; Huang, Y.; Zhang, D.; Zhu, Y.; Sun, Z.; Luo, T. Characteristics of Vein-Forming Fluids in the Sinian Dengying Formation Reservoir and Its Relationship with the Hydrocarbon Accumulation Process in the Southwest and Southeast of the Sichuan Basin. *Minerals* **2022**, *12*, 443. <https://doi.org/10.3390/min12040443>

Academic Editor:
Leszek Marynowski

Received: 3 March 2022

Accepted: 2 April 2022

Published: 3 April 2022

Publisher's Note: MDPI stays neutral with regard to jurisdictional claims in published maps and institutional affiliations.



Copyright: © 2022 by the authors. Licensee MDPI, Basel, Switzerland. This article is an open access article distributed under the terms and conditions of the Creative Commons Attribution (CC BY) license (<https://creativecommons.org/licenses/by/4.0/>).

Abstract: Multistage fluid activities and hydrocarbon accumulation processes have occurred in the Dengying Formation of the Sichuan Basin during its long geological history. Petrography and cathodoluminescence observations; in situ microanalysis of rare earth elements, carbon, oxygen, and strontium isotopes; fluid inclusion microthermometric experiments; laser Raman experiments; burial history; thermal history; and hydrocarbon generation history simulation have been applied to study the characteristics of vein-forming fluid in the Dengying Formation reservoirs in the southeast and southwest of Sichuan Basin and to analyze in-depth the multistage fluid activity and hydrocarbon accumulation process. The results show that two stages of dolomite and one stage of quartz are developed in the 4th member of the Dengying Formation in the southeast of Sichuan Basin, and three stages of dolomite are developed in the 2nd member of the Dengying Formation in the southwest of Sichuan Basin. The source of the dolomite veins is mainly reservoir marine diagenetic fluid. Dolomites developed in the Hercynian period were affected by hydrothermal activity to a certain extent which may have been caused by the activity of the Emei mantle plume. The diagenetic mineral sequence of the 4th member of the Dengying Formation in the southeast of Sichuan Basin is quartz (432 Ma)/dolomite I (421 Ma)/dolomite II (288 Ma), and the 2nd member of the Dengying Formation in the southwest of the Sichuan Basin is dolomite I (425 Ma)/dolomite II (283 Ma)/dolomite III (262 Ma). The main hydrocarbon accumulation period was during the Hercynian–Indosinian stage which was related to the thermal influence of the Emei mantle plume activity on the source rock of the Qiongzhusi Formation. Combined with petrography, inclusion thermometry, burial history, and hydrocarbon generation history simulation, the fluid activity and hydrocarbon accumulation evolution sequence in the southeast and southwest of the Sichuan Basin are determined comprehensively.

Keywords: dolomite veins; rare earth element (REE); source of vein-forming fluid; hydrocarbon accumulation process; Dengying Formation; Sichuan Basin

1. Introduction

In recent years, with the further progress of petroleum exploration, natural gas resources in the deep strata have become a hot spot in the field of oil and gas exploration [1–5]. In the central area of the Sichuan Basin, the industrial gas resources of the deep Cambrian strata have been discovered which are represented by the Anyue and Moxi gas fields [6–10].

The exploration of marine carbonate strata in the lower combination formation in the southeast of the Sichuan Basin has been occurring for a long period of time [11–14]. The Dingshan, Lintanchang, and Ximen assemblage traps have been found, and many wells have been drilled. The formation of the lower assemblage of the Dengying Formation has been difficult to research due to its very old age and large burial depth [15–17]. The dolomite reservoir of the Sinian Dengying Formation has experienced multiperiod tectonic movements, accompanied by multiperiod diagenetic fluid activities [12,14,18–20]. The Dengying Formation has experienced large-scale tectonic uplift and overbearing strata erosion in the Yanshan and Himalayan periods, and the oil and gas reservoirs of the Dengying Formation has been reformed, adjusted, and even destroyed [12,21,22].

Previous studies on the Dengying Formation in the southwest and southeast of the Sichuan Basin have provided a certain understanding of the hydrocarbon accumulation process in the study area [12,23–26]. At the same time, some scholars have analyzed the paleo-fluid activity and characteristics of the reservoir in the Dengying Formation to a certain extent [18,27–30]. However, there is a lack of an overall study on the hydrocarbon accumulation process and multistage paleo-fluid activities from macro- to microscopic veins. In addition, the establishment of multistage diagenetic fluid sequence, paleo-fluid activity, the difference in paleo-temperature and pressure conditions, and a dynamic evaluation of the hydrocarbon accumulation process in the Dengying Formation of Sichuan Basin have not been systematically studied. The characteristics and information of the paleo-fluid activity in the reservoir can be used to indicate the accumulation and destruction of oil and gas [31–35]. In this paper, we analyze the veins of the dolomite reservoir in the Dengying Formation of the Lin 1 well in the Lintanchang area in the southeast of the Sichuan Basin and the Jinshi 1 well in the Jinshi structure in the southwest of the Sichuan Basin (Figure 1). The paleo-fluid activity stages, sources, and forming environments are studied by means of micropetrography; cathodoluminescence; rare earth elements (REEs); carbon, oxygen and strontium isotopes; and fluid inclusions, to provide important information for the study of the hydrocarbon accumulation process.

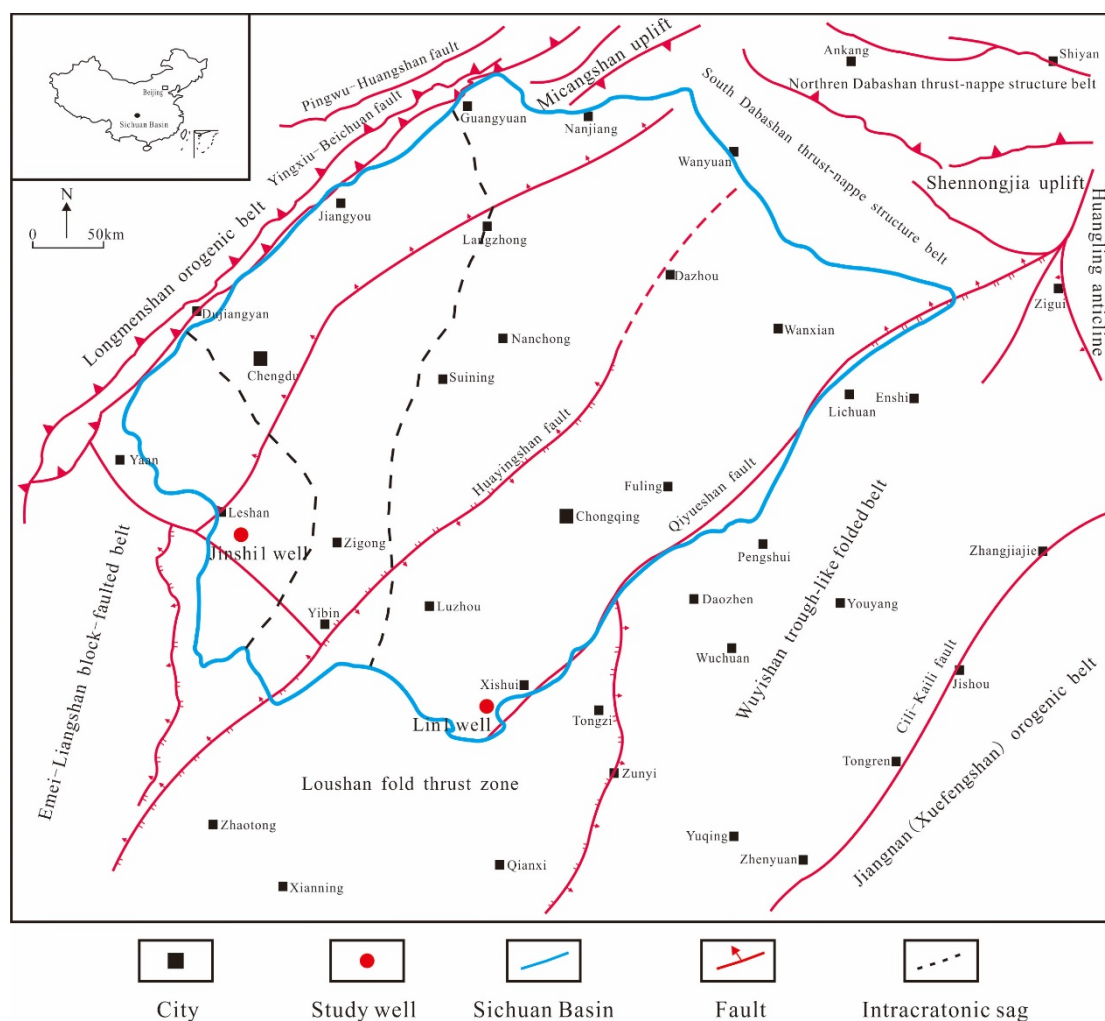


Figure 1. Regional geological map and well location map of the Sichuan Basin.

2. Geological Background

The Sichuan Basin is a large petroleum superposed basin, and many years of oil and gas exploration have shown that it contains rich oil and gas resources [6,36–38]. The study area is located in the high steep fold belt in eastern Sichuan Basin and the middle-low steep fold belt in southern Sichuan Basin [12,39]. The lower assemblage strata with a geological age of approximately 542–419 Ma (from the Sinian to the Silurian systems) in this area have developed several sets of high-quality source-reservoir-caprock assemblages vertically, which have been new targets for natural gas exploration in recent years (Figure 2) [38,40–42]. The Sinian Dengying Formation, as one of the main reservoirs, has attracted extensive attention. The Sinian Dengying Formation is one of the oldest oil and gas reservoirs in the world. It is characterized by its old age, large burial depth, and long geological history, which leads to its complex petrogenetic evolution process [15,17,43]. From the bottom to top, the Dengying Formation can be divided into four members: the 1st member (Z_2dn^1), the 2nd member (Z_2dn^2), the 3rd member (Z_2dn^3) and the 4th member (Z_2dn^4). The lithology of Z_2dn^1 is mainly dark gray and gray microcrystal dolomite, and algal-laminated dolomite is locally developed. The Z_2dn^2 is rich in algae, and the lithology is mainly a light gray thick layer of algal-laminated dolomite, with local powder crystal dolomite. The lithologic color of the Z_2dn^3 is relatively shallow, mainly consisting of light gray algal-laminated dolomite and powder-microcrystalline dolomite, and a small amount of silicified dolomite or silicalite can be seen locally. The lithology of the Z_2dn^4 is mainly a light gray thick-layered powder-fine crystal dolomite and algal dolomite, and the top surface is partially medium-coarse

crystal dolomite [14,28,44]. The sedimentary facies of the Dengying Formation are mainly shallow marine carbonate platform facies (mainly intertidal zone and tidal-flat subfacies), which are rich in algal organisms [45,46]. The sedimentary water energy of the Dengying Formation has gradually transferred from the higher energy intertidal zone to the lower energy environment of the lagoon. The changes in the lithology of the Dengying Formation also reflect this transformation of water energy. The Dengying Formation in the south of the Sichuan Basin has undergone complex tectonic evolution [12,39,47], mainly including an uplift and erosion in Late Sinian, a subsidence in Early Paleozoic, an uplift and erosion stage from Late Silurian to Carboniferous, a subsidence from Permian to Late Cretaceous, and a rapid uplift from Late Cretaceous to now. These complex geological tectonic activities resulted in the active formation fluid of the Dengying Formation, and the evolution of the reservoir and the condition of oil and gas preservation conditions have been significantly adjusted and reformed [25].

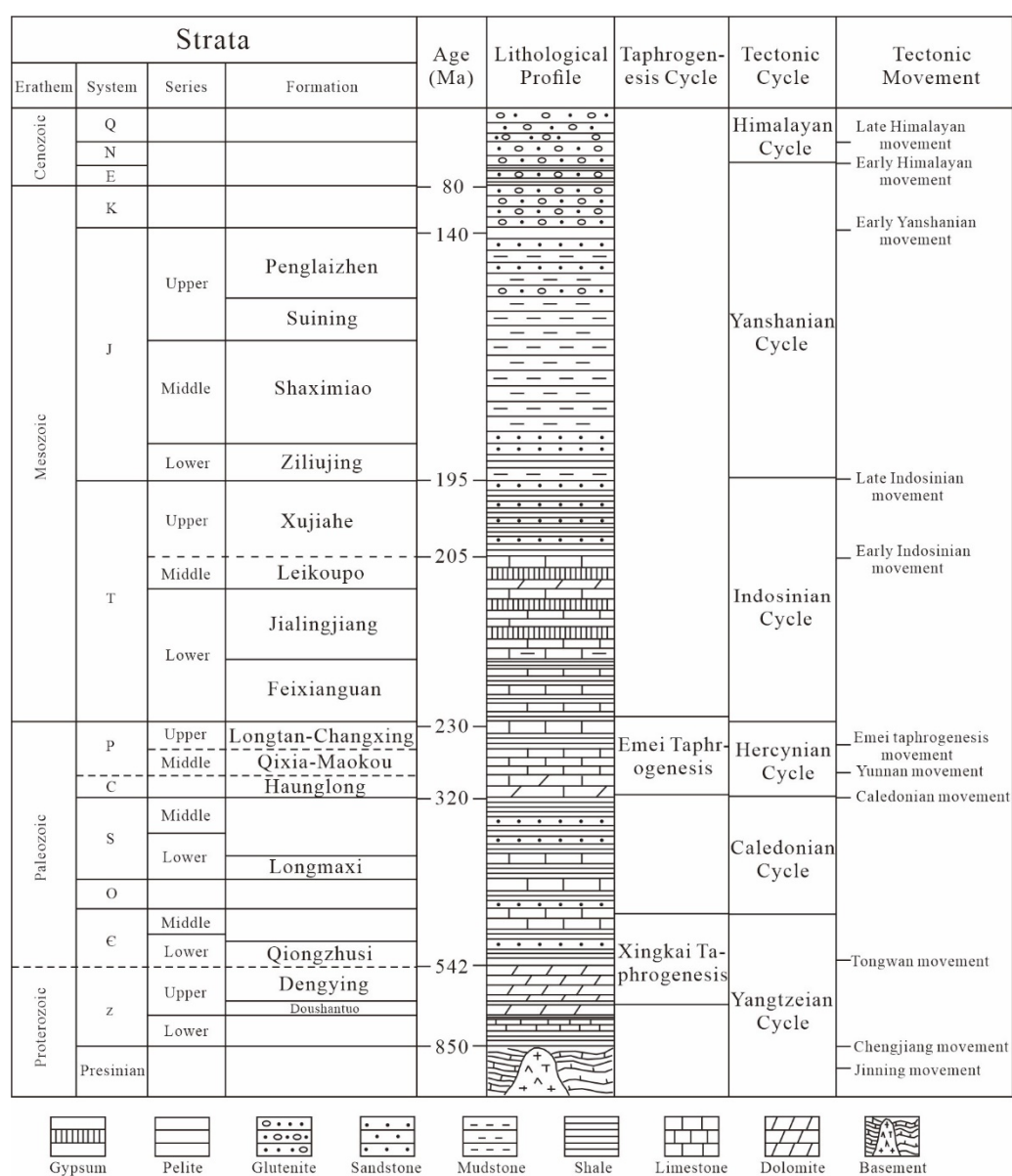


Figure 2. Stratigraphic and tectonic event map of the Sichuan Basin (modified after Liu et al., 2018).

3. Samples and Methods

In this study, vein-bearing carbonate rock samples were selected from two wells in the southeast and southwest of the Sichuan Basin, of which 4 vein filling samples from the 4th member of the Dengying Formation of the Lin 1 well in the southeast of the Sichuan Basin and 3 vein filling samples from the 2nd member of the Dengying Formation of the Jinshi 1 well in the southwest of the Sichuan Basin were selected. One source rock sample of the Qiongzhusi Formation from the Lin 1 well and two source rocks of the Qiongzhusi Formation from the Jinshi 1 well were selected (Figure 3).

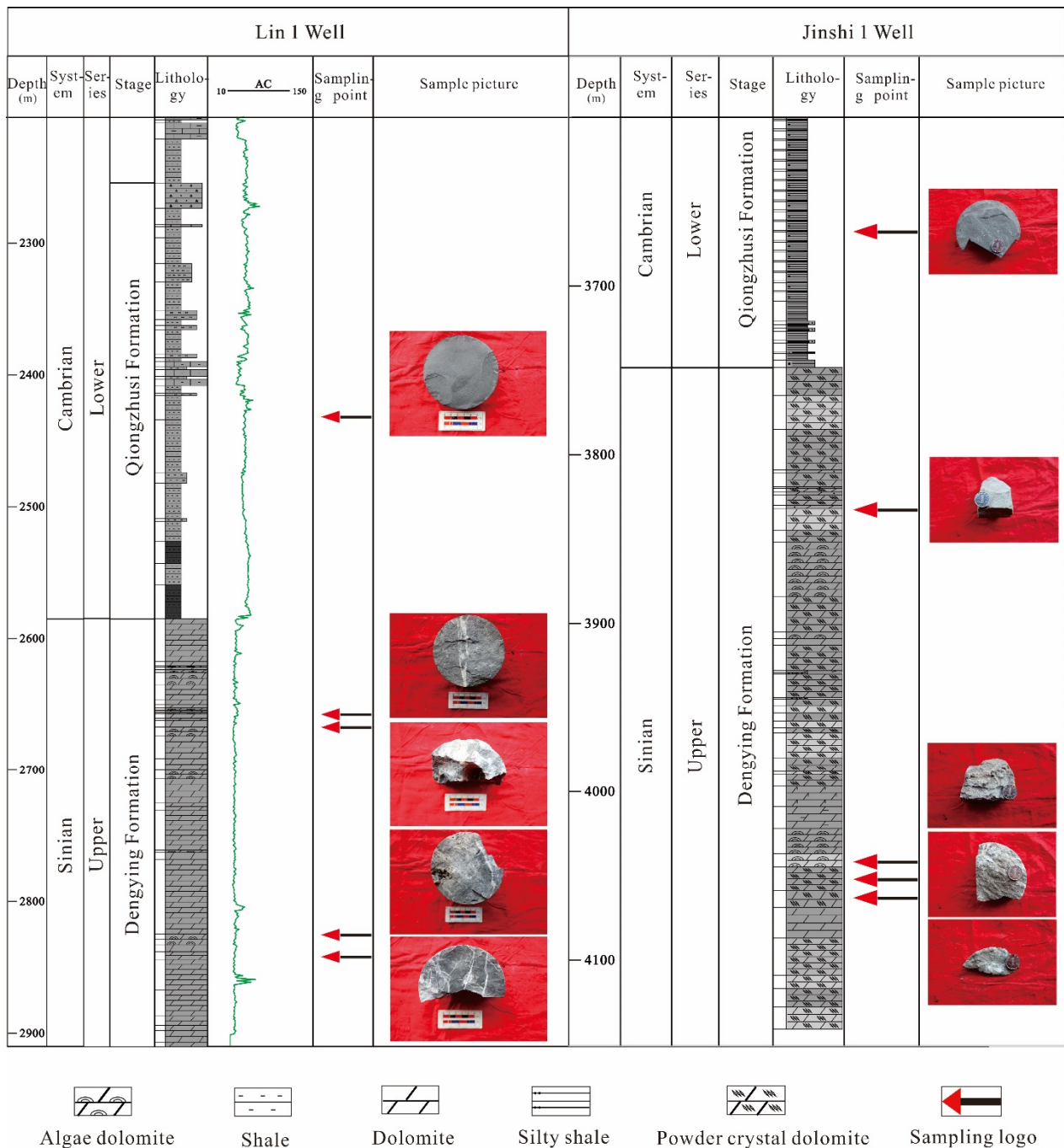


Figure 3. Comprehensive bar chart and core sampling locations of the Dengying Formation at the Lin 1 well and the Jinshi 1 well.

The samples were made into 100 μm thick, double-sided polished microsections and observed under a Leica microscope. The cathodoluminescence analysis was carried out with a CL8200-MK5 cathodoluminescence instrument. The test conditions were 0.3 Pa, the beam voltage was 11 kV, and the beam current was 300 μA .

The temperature of fluid inclusions was measured using double-sided polished microsections with a thickness of 100 μm and the test instrument was a Zeiss Axio Scope. A1 double-channel fluorescence and a transmission light microscope were combined with a LinkAM-THMSG600 hot and cold platform; the error of the hot and cold platform was ± 0.1 $^{\circ}\text{C}$ after correction. During temperature measurement process, the heating rate was controlled between 0.1 and ~ 5 $^{\circ}\text{C}/\text{min}$. The inclusion temperatures were observed and recorded when the inclusions were completely homogenized, and the ice was completely melted. The homogenization temperature and freezing point of the brine inclusions were measured.

LA-ICP-MS was used for the microanalysis of the content of elements at the calibration points on the veins. For each point, the diameter of the laser beam spot was 120 μm , the background signal acquisition time was 25 s, and the measurement time was 50 s. The standard sample for the in situ microanalysis of elements was artificial silicate glass NIST610, and the standard sample was re-tested at every 8 points measured. The content of Ca element in the standard sample was taken as the internal standard for the content calculation. The offline processing of the analyzed data was completed by ICPMS-DataCal.

The carbon, oxygen, and strontium isotope tests were conducted at the Key Laboratory of Tectonics and Petroleum Resources, Ministry of Education and State Key Laboratory, China University of Geosciences, Wuhan. The pure carbonate vein samples (dolomite or calcite) separated from the surrounding host rocks were broken into about 200 mesh powder, and reacted with orthophosphoric acid at 25 $^{\circ}\text{C}$ for 1 d to extract carbon dioxide for the carbon and oxygen isotope analyses. The analyses are reported in per mol relative to Vienna Pee Dee Belemnite (V-PDB) for carbon and oxygen with analytical uncertainties of better than ± 0.1 ‰ (1σ).

A LabRAM HR800 microlaser Raman spectrometer (HORIBA Jobin Yvon S.A.S) was used to conduct the fluid inclusion laser Raman experiment. The test ambient temperature was 25–230 $^{\circ}\text{C}$, the light source was YAG laser, the wavelength was 532.06 nm, the output power was 350–400 mW, the line width was <0.1 nm, the power of the laser beam on the surface of the sample was generally 60–80 mW, and the confocal effect of the spectrometer could reach the spatial resolution of 0.1 μm in the transverse direction and 0.3 μm in the depth direction. A silicon standard sample with a Raman peak displacement of 520.70 cm^{-1} was used for wave value correction of the instrument. The time of single data acquisition was generally 10–20 s, and 20–70 times of stacking.

The BasinMod-1D software was used to simulate the burial history, thermal history, and mature hydrocarbon generation history. Based on logging lithology and stratification data, the reciprocal compaction model was used to recover the thickness of strata in different geological periods, and then the burial history was simulated. The BasinMod-1D software default values were used for the initial porosity and compaction factor of pure lithology. By counting the percentage of pure lithology in each layer and calculating the arithmetic average value of each parameter, the assignment of mixed lithology parameters was realized. Based on the burial history and thermal history simulation, the maturation and hydrocarbon generation history of the Qiongzhusi Formation source rock was recovered.

4. Results

4.1. Petrographic Characteristics

The pore, cavity, and fracture of carbonate reservoir in the 4th member of the Sinian Dengying Formation in the Lin 1 well in the southeast of the Sichuan Basin are filled with complex multistage minerals. The veins are mainly filled with carbonate minerals, which are generally filled with multistage dolomite. Some amount of clastic quartz is found within veins (Figure 3). The veins of the 2nd member of the Dengying Formation in the Jinshi 1 well in the southwest of the Sichuan Basin are mainly distributed in the dissolution

cavities (Figure 3). The overall performance of the veins is similar to that of the Lin 1 well, which are filled with multistage dolomite.

According to the observations of core sample and thin section under microscope, the veins of the reservoir in the 4th member of the Dengying Formation of the Lin 1 well are mainly fracture-cavity filling type. The veins are mostly distributed in the surrounding rock in strips, and the widths of veins are different which are distributed in the range of 1~5 mm (Figure 3). In addition, dolomite and quartz are also found in dissolution pores in core samples. Thin section microscopic observations showed significantly different occurrence developments in the vein body sizes of multistage dolomite (Figure 4A,C). The cathodoluminescence of the thin section in the Lin 1 well shows that two stages of dolomite (dolomite I and dolomite II) and one stage of quartz are developed in the 4th member of the Dengying Formation. Dolomite I is in contact with the surrounding rock, and the cathodoluminescence color is dark red or close to no luminescence. Dolomite II mineral particles are massive coarse grained and in contact with the first stage dolomite, and the cathodoluminescence color is bright red (Figure 4A,B). At the same time, quartz and dolomite are filled in the pores under the observation of a thin section (Figure 4C). The cathodoluminescence shows that quartz does not emit light, the dolomite shines red, and asphalt is filled in the pores between quartz and dolomite (Figure 4D,E). In addition, dolomite is developed inside the strip quartz vein, the quartz vein is in contact with the surrounding rock, and the dolomite grows and develops in the middle of the quartz. The cathodoluminescence shows that the quartz vein does not emit light, and the dolomite shines red (Figure 4F,G).

The reservoir veins of the 2nd member of the Dengying Formation in the Jinshi 1 well in the southwest of the Sichuan Basin are mainly filled in solution pores, and the dolomite grains are developed in the dissolution cavities of reservoirs (Figure 3). The dissolution pores in the reservoir of the 2nd member of the Dengying Formation in the Jinshi 1 well are obviously filled with multistage minerals which are mainly dolomite. Ordinary microscopic observations and cathodoluminescence observations of the 2nd member of the Dengying Formation in the Jinshi 1 well in the southwest of the Sichuan Basin show that three different stages of dolomite are developed (Figure 5A,D,G). Dolomite I is a ring of banded dolomite, which was deposited in the early syngenetic period and does not emit light under cathodoluminescence (Figure 5C,E,H). Dolomite II and dolomite III are coarse-grained dolomites, and Dolomite II does not glow under cathodoluminescence, while Dolomite III emits red light (Figure 5C,E,H). Coarse-grained dolomite is found in the outer ring banded algal dolomite in several thin sections (Figure 5F). At the same time, liquid oil (asphalt at present) filling can be seen in the pores between the filled coarse-grained dolomite mineral grains (Figure 5I).

4.2. Rare Earth Elements (REEs)

Rare earth elements can be used to classify the formation stages of veins, and the properties and sources of fluids can be inferred from the morphology of rare earth element distribution patterns [48–51].

The total REE concentration of the Lin 1 well ranges from 0.056 ppm to 0.558 ppm with an average of 0.273 ppm, and the total REE contents in the Jinshi 1 well ranges from 0.022 ppm to 0.825 ppm, with an average value of 0.280 ppm (Table 1). In the REE distribution of the vein body of the Lin 1 well in the southeast of the Sichuan Basin, the LREE/HREE ratio ranges from 0.388 to 0.590, and the average value is 0.509, and in the Jinshi 1 well, the LREE/HREE ratio ranges from 0.965 to 1.352, and the average value is 1.151. The REE distributions of the Lin 1 and Jinshi 1 wells show negative Ce anomaly (Figure 6), of which the δCe ($\delta\text{Ce} = \text{Ce}/((\text{La} + \text{Pr})/2) \text{ N}$, N = normalized value by PAAS) of the Lin 1 well ranges from 0.457 to 0.747 with an average value of 0.604, and that of the Jinshi 1 well ranges from 0.482 to 0.798 with an average value of 0.584. The rare earth elements in the vein body of the Lin 1 and Jinshi 1 wells present positive Eu anomaly in general (Figure 6), of which the δEu ($\delta\text{Eu} = \text{Eu}/((\text{Sm} + \text{Gd})/2) \text{ N}$, N = normalized value

by PAAS) distribution ranges from 0.765 to 1.628 in the Lin 1 well, and the vein body of the Jinshi 1 well also shows positive Eu anomaly with the δEu ranging from 0.894 to 1.753 (Table 1).

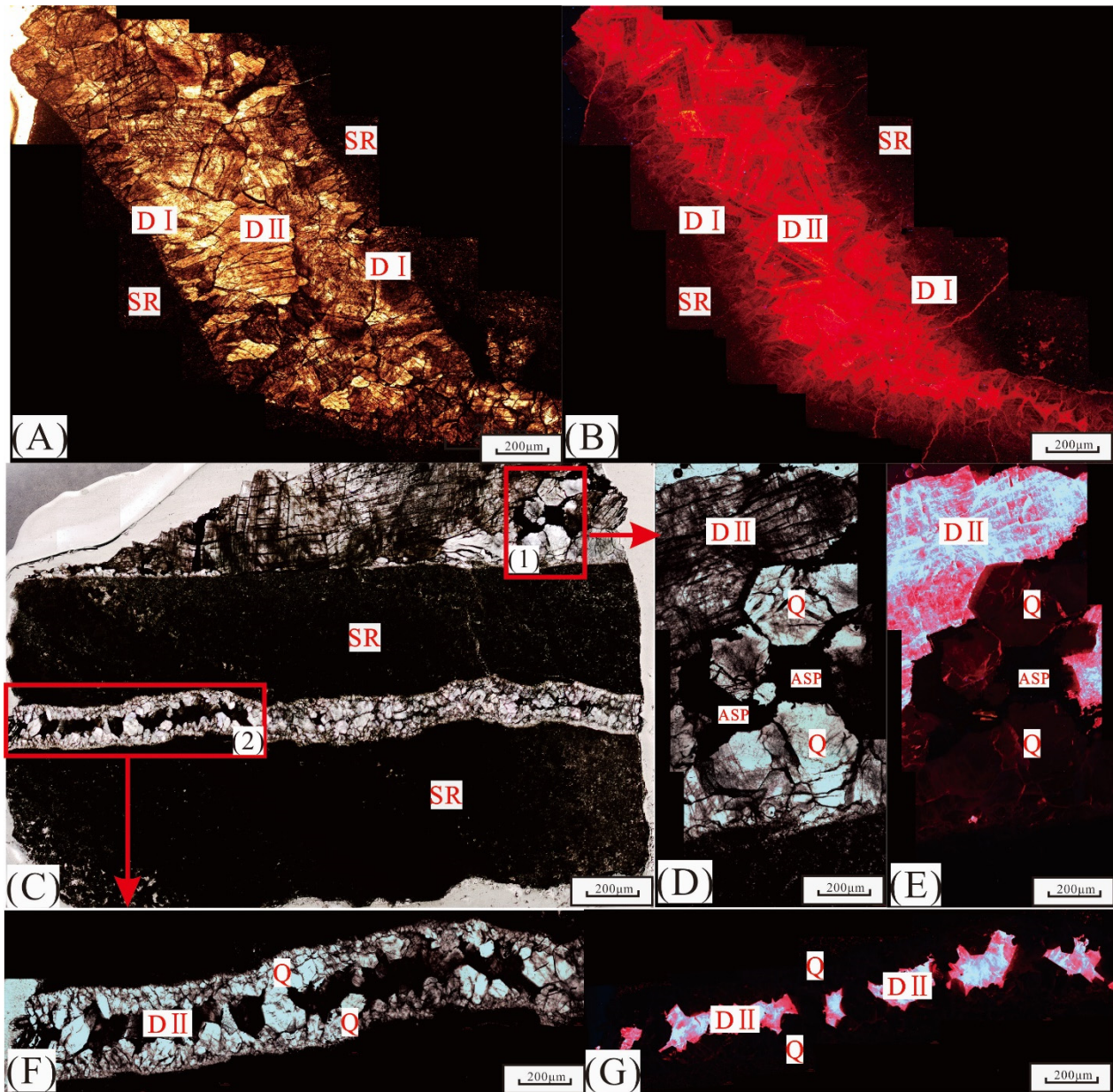


Figure 4. Petrography and cathodoluminescence characteristics of the 4th member of the Dengying Formation filled with dolomite and quartz minerals and asphalt in the Lin 1 well (DI, DII, Q, and ASF are dolomite I, dolomite II, quartz, and asphalt, respectively): (A) Dolomite veins panoramic photograph of plane polarized light, 2826.29 m; (B) dolomite veins panoramic photograph of cathodoluminescence, 2826.29 m; (C) inclusion thin section panoramic photograph of plane polarized light, 2647.20 m; (D) partial enlargement of area (1) in photograph (C), 2647.20 m; (E) cathodoluminescence photograph of partial enlargement of area (1) in photograph (C), 2647.20 m; (F) partial enlargement of area (2) in photograph (C), 2647.20 m; (G) cathodoluminescence photograph of partial enlargement of area (2) in photograph (C), 2647.20 m.

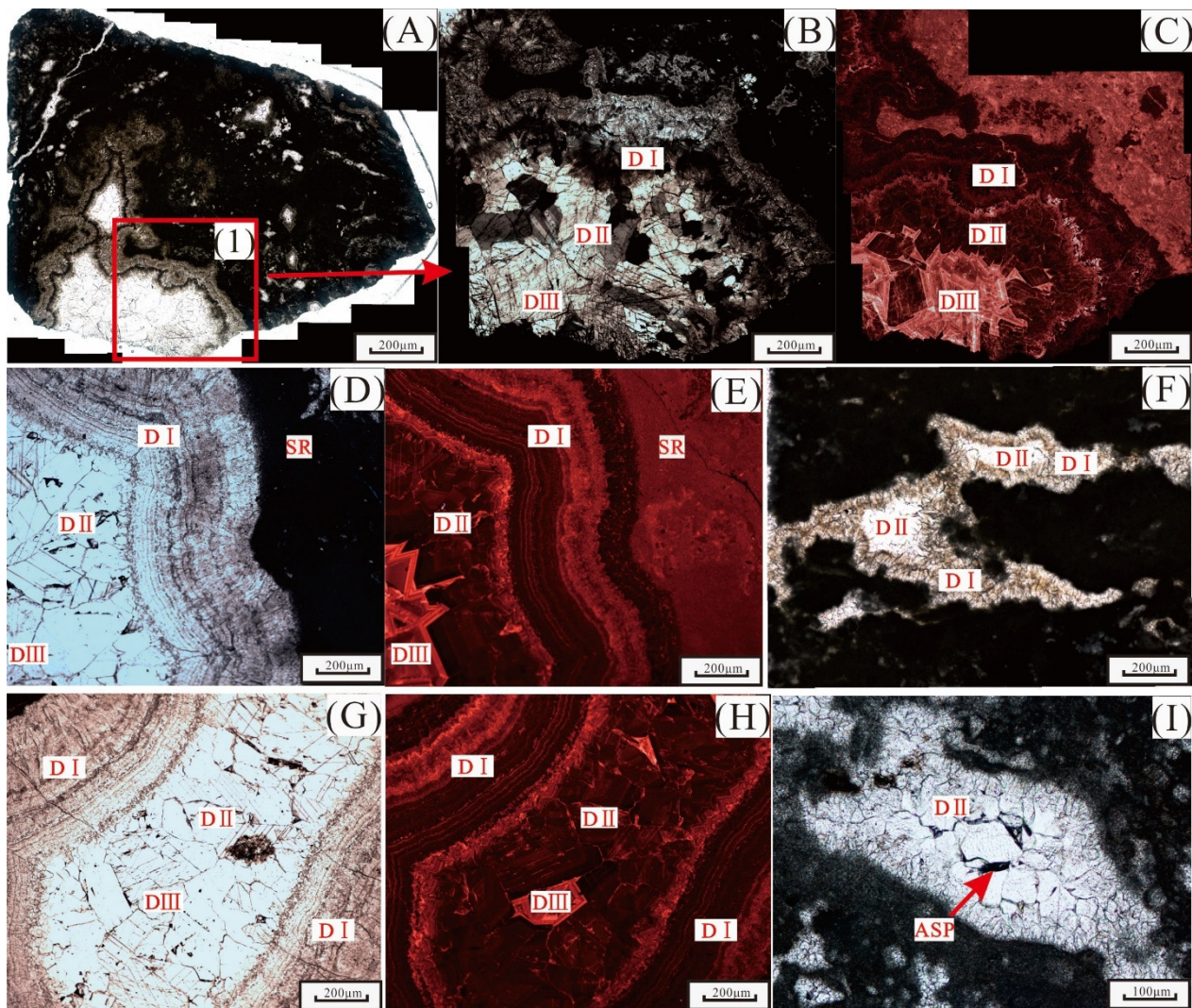


Figure 5. Petrography and cathodoluminescence characteristics of the 2nd member of the Dengying Formation filled with dolomite minerals and asphalt in the Jinshi 1 well (DI, DII, DIII, and ASP are dolomite I, dolomite II, dolomite III, and asphalt, respectively): (A) Inclusion thin section panoramic photograph of plane polarized light, 4027.54 m; (B) local enlarged panoramic photograph of area 1 in (A), 4027.54 m; (C) local enlarged panoramic photograph of area 1 in (A) of cathodoluminescence, 4027.54 m; (D) inclusion thin section photograph of plane polarized light, 4028.74 m; (E) inclusion thin section photograph of cathodoluminescence, 4028.74 m; (F) photograph of dolomite of different occurrences in the 2nd member the Dengying Formation, 4028.74 m; (G) inclusion thin section photograph of plane polarized light, 4029.21 m; (H) inclusion thin section photograph of cathodoluminescence, 4029.21 m; (I) inclusion thin section photograph of plane polarized light, 4032.50 m.

Table 1. Rare earth element (REE) concentrations of dolomite veins in the Dengying Formation in the Lin 1 and Jinshi 1 wells.

Sample	Well	Rare Earth Element (ppm)														Σ REE (ppm)	LREE/HREE	δ Eu	δ Ce	Y/Ho
		La	Ce	Pr	Nd	Sm	Eu	Gd	Tb	Dy	Ho	Er	Tm	Yb	Lu					
JS-4-01	Jinshi 1	0.003	0.002	0.002	0.002	0.001	0.001	0.002	0.002	0.001	0.002	0.001	0.001	0.000	0.000	0.022	1.328	0.894	0.564	40.625
JS-4-02	Jinshi 1	0.013	0.010	0.016	0.018	0.013	0.024	0.020	0.016	0.012	0.014	0.009	0.009	0.006	0.008	0.187	0.990	1.495	0.665	49.180
JS-4-03	Jinshi 1	0.058	0.037	0.073	0.084	0.075	0.121	0.086	0.062	0.057	0.050	0.042	0.035	0.022	0.021	0.825	1.192	1.507	0.562	53.599
JS-4-05	Jinshi 1	0.012	0.009	0.022	0.026	0.029	0.046	0.030	0.022	0.021	0.021	0.015	0.016	0.009	0.009	0.286	1.019	1.552	0.552	48.186
JS-4-06	Jinshi 1	0.014	0.006	0.010	0.010	0.009	0.009	0.010	0.010	0.010	0.008	0.006	0.005	0.003	0.006	0.116	0.965	0.909	0.534	52.276
JS-5-01	Jinshi 1	0.009	0.003	0.004	0.005	0.005	0.006	0.006	0.004	0.003	0.003	0.006	0.002	0.002	0.003	0.062	1.092	1.114	0.518	65.148
JS-5-02	Jinshi 1	0.006	0.002	0.004	0.004	0.003	0.005	0.003	0.003	0.002	0.002	0.002	0.003	0.002	0.003	0.043	1.352	1.643	0.482	79.693
JS-8-02	Jinshi 1	0.033	0.035	0.054	0.063	0.071	0.132	0.079	0.058	0.048	0.042	0.031	0.020	0.015	0.014	0.696	1.266	1.753	0.798	40.185
L-11-02	Lin 1	0.003	0.003	0.004	0.005	0.006	0.006	0.008	0.008	0.006	0.008	0.008	0.006	0.007	0.004	0.082	0.492	0.765	0.747	32.651
L-11-03	Lin 1	0.004	0.003	0.005	0.006	0.008	0.009	0.009	0.009	0.011	0.013	0.008	0.005	0.008	0.004	0.102	0.510	1.156	0.693	24.537
L-12-01	Lin 1	0.005	0.002	0.002	0.002	0.004	0.006	0.008	0.004	0.006	0.005	0.004	0.002	0.002	0.004	0.056	0.568	1.024	0.457	51.373
L-12-03	Lin 1	0.007	0.003	0.005	0.006	0.009	0.009	0.007	0.008	0.010	0.013	0.011	0.009	0.006	0.006	0.110	0.561	1.100	0.466	35.785
L-13-01	Lin 1	0.009	0.007	0.014	0.020	0.027	0.049	0.047	0.042	0.054	0.052	0.042	0.042	0.028	0.020	0.455	0.388	1.329	0.607	35.166
L-13-02	Lin 1	0.010	0.009	0.019	0.025	0.028	0.062	0.048	0.045	0.054	0.058	0.048	0.045	0.038	0.022	0.512	0.428	1.628	0.597	35.610
L-13-03	Lin 1	0.010	0.007	0.015	0.017	0.021	0.039	0.028	0.030	0.032	0.034	0.027	0.022	0.019	0.010	0.311	0.538	1.597	0.595	33.636
L-13-04	Lin 1	0.012	0.014	0.030	0.037	0.046	0.068	0.067	0.051	0.058	0.058	0.042	0.029	0.026	0.021	0.558	0.590	1.218	0.667	34.526
PAAS		38.2	79.6	8.83	33.09	5.55	1.08	4.66	0.774	4.68	0.991	2.85	0.405	2.82	0.433					

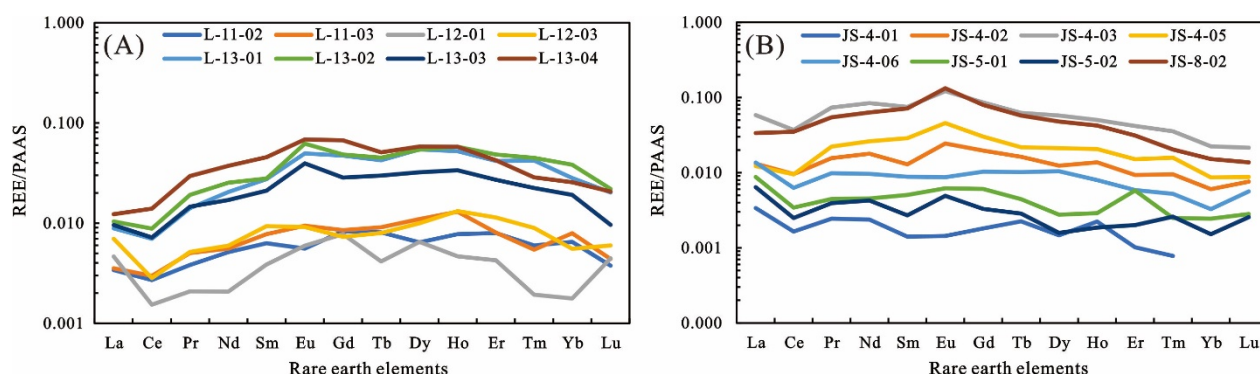


Figure 6. Distributions of rare earth elements in dolomite of the Lin 1 well (A) and the Jinshi 1 well (B). The concentrations are normalized to the PAAS.

4.3. Carbon, Oxygen, and Strontium Isotopes

The $\delta^{13}\text{C}_{\text{PDB}}$ values of the carbonate reservoir veins in the Lin 1 well are between 0.42‰ and 2.46‰ with an average of 1.67‰, and the $\delta^{18}\text{O}_{\text{PDB}}$ values are between −12.81‰ and −11.75‰ with an average of −12.30‰. In addition, the $\delta^{13}\text{C}_{\text{PDB}}$ value of the surrounding rock is 3.06‰ and the $\delta^{18}\text{O}_{\text{PDB}}$ value is −10.21‰. For the Jinshi 1 well, the $\delta^{13}\text{C}_{\text{PDB}}$ values of the vein body range from 2.66‰ to 2.82‰ with an average of 2.75‰, and the $\delta^{18}\text{O}_{\text{PDB}}$ values ranges from −10.34‰ to −9.63‰ with an average of −10.02‰. The $\delta^{13}\text{C}_{\text{PDB}}$ and $\delta^{18}\text{O}_{\text{PDB}}$ values of the surrounding rock of the Jinshi 1 well are 3.70‰ and −5.56‰, respectively. The strontium isotope $^{87}\text{Sr}/^{86}\text{Sr}$ of the vein body of the Lin 1 well is distributed between 0.711359 and 0.714824 with an average value of 0.712524, and the value $^{87}\text{Sr}/^{86}\text{Sr}$ of the surrounding rock is 0.709935. The $^{87}\text{Sr}/^{86}\text{Sr}$ ratio of the vein body of the Jinshi 1 well varies from 0.709030 to 0.710144 with an average value of 0.709497, while it is 0.709724 for the surrounding rock (Table 2). The values of carbon and oxygen isotopes in dolomite of the 4th member of the Dengying Formation in the Lin 1 well are lower than those of surrounding rock. The carbon and oxygen isotope values of the dolomite in the 2nd member of the Dengying Formation of the Jinshi 1 well show similar characteristics and are lower than those of surrounding rock. However, the carbon and oxygen isotope values of the dolomite in the 4th member of the Dengying Formation in the Lin 1 well are lower than those of the dolomite in the 2nd member of the Dengying Formation in the Jinshi 1 well, showing a negative deviation to a certain extent. The difference between the carbon and oxygen isotope values of the dolomite in the 2nd member of the Dengying Formation in the Jinshi 1 well and the surrounding rock is larger than those between the dolomite in the 4th member of the Dengying Formation in the Lin 1 well and the surrounding rock, and the oxygen isotope values of the dolomite are more negative than those of the surrounding rock. The strontium isotope values of the dolomite in the 4th member of the Dengying Formation in the Lin 1 well are all higher than those of the surrounding rock, and there is little difference between the strontium isotope values of the dolomite in the 2nd member of the Dengying Formation in the Jinshi 1 well and those of surrounding rock, except for one dolomite sample whose strontium isotope values are higher than those of the surrounding rock. The strontium isotope of the dolomite in the 4th member of the Dengying Formation in the Lin 1 well is generally higher than that in the 2nd member of the Dengying Formation in the Jinshi 1 well.

Table 2. Carbon, oxygen, and strontium isotope compositions of dolomite veins and surrounding rock of the 4th member of the Dengying Formation in the Lin 1 well and the 2nd member of the Dengying Formation in the Jinshi 1 well.

Sample	Well	Type	Depth	$\delta^{13}\text{C}_{\text{PDB}}$	$\delta^{18}\text{O}_{\text{PDB}}$	$^{87}\text{Sr}/^{86}\text{Sr}$	$\delta^{18}\text{O}_{\text{SMOW}}$
L-1	Lin 1	Dolomite I	2654.30	0.42	−12.35	0.714824	18.18
L-2	Lin 1	Dolomite I	2826.29	2.13	−12.81	0.711359	17.70
L-3	Lin 1	Dolomite I	2831.41	2.46	−11.75	0.711389	18.80
Lin1-W	Lin 1	Surrounding rock	2831.41	3.06	−10.21	0.709935	20.38
JS-1	Jinshi 1	Dolomite III	4028.74	2.77	−9.63	0.709030	20.98
JS-2	Jinshi 1	Dolomite III	4029.21	2.82	−10.34	0.709317	20.24
JS-3	Jinshi 1	Dolomite I	4032.50	2.66	−10.09	0.710144	20.51
Jinshi1-W	Jinshi 1	Surrounding rock	4032.50	3.70	−5.56	0.709724	25.17

4.4. Characteristics of Fluid Inclusions

A large number of fluid inclusions are present in the carbonate reservoir veins of the Dengying Formation in the Lin 1 well in the southeast of the Sichuan Basin and the Jinshi 1 well in the southwest of the Sichuan Basin, which are mainly gas-liquid two-phase brine inclusions (Inclusion I) and a small amount of single-phase methane inclusions (Inclusion II). A small amount of methane-bearing brine inclusions (Inclusion III) is also developed. Methane inclusions have a lens-concentrating effect, which means they appear black at the edge and bright white at the middle when viewed under a transmission light microscope [52,53]. Primary brine inclusions are mainly developed in the dolomite minerals of the Dengying Formation in the Lin 1 well, which are oval and irregular in shape with a long axis size of 6–21 μm . In addition to the primary brine inclusions, a few methane-bearing brine inclusions are also developed (Figure 7A). Methane inclusions are developed in quartz minerals that are irregular in shape with long axis sizes of 3–8 μm and are associated with brine inclusions (Inclusion I) (Figure 7C), which were captured in the same period as methane inclusions. The secondary methane inclusions are mostly irregular and elliptical in shape with a linear mass aggregation distribution and a long axis of 4–15 μm (Figure 7B). A large number of brine inclusions, and a small amount of methane inclusions and methane-bearing brine inclusions are developed in dolomite minerals of the Dengying Formation in the Jinshi 1 well. Most brine inclusions are approximately round or irregular in shape and small in volume, with a long axis size of 3–7 μm (Figure 7E). Some brine inclusions are linear distribution and are secondary brine inclusions (Figure 7D), which may have been formed by later fluid charging. The quantity of pure methane inclusions in dolomite minerals of the Dengying Formation in the Jinshi 1 well is small and the shapes of the inclusions are small, with long axis sizes of about 2 μm (Figure 7F). However, the quantity of methane-bearing brine inclusions in dolomite minerals is large (Figure 7D).

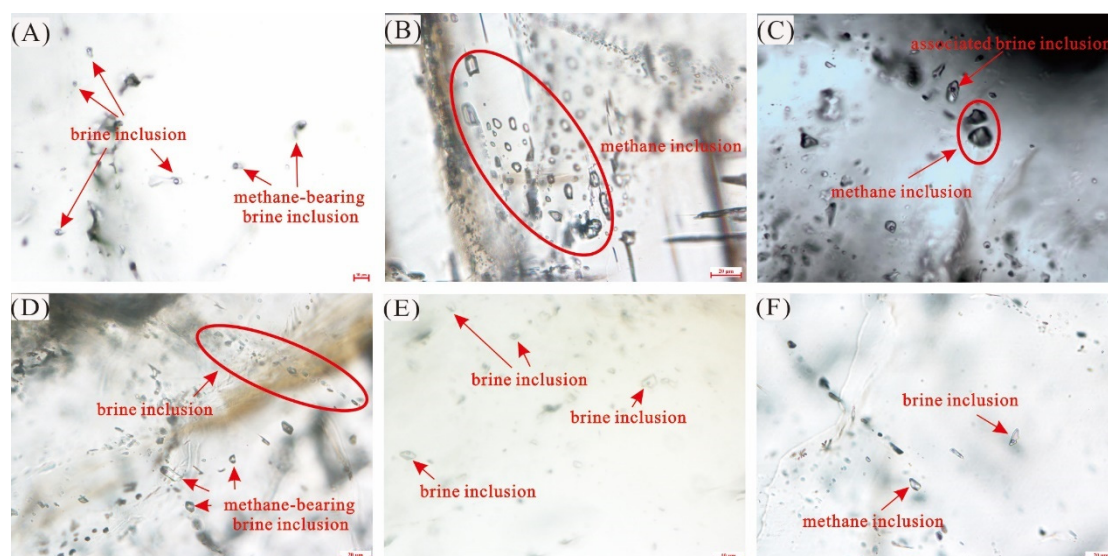


Figure 7. Petrography of fluid inclusions in the Dengying Formation of the Lin 1 and Jinshi 1 wells: (A) Brine inclusions and methane-bearing brine inclusions developed in dolomite of the 4th member of the Dengying Formation in the Lin 1 well, 2826.29 m; (B) secondary methane inclusions in the quartz of the 4th member of the Dengying Formation in the Lin 1 well, 2657.37 m; (C) secondary methane inclusions associated with brine inclusions in the quartz of the 4th member of the Dengying Formation in the Lin 1 well, 2657.37 m; (D) brine inclusions and methane-bearing brine inclusions developed in the dolomite of the 2nd member of the Dengying Formation in the Jinshi 1 well, 4027.54 m; (E) brine inclusions developed in the dolomite of the 2nd member of the Dengying Formation in the Jinshi 1 well, 4028.74 m; (F) brine inclusions and methane inclusions developed in the dolomite of the 2nd member of the Dengying Formation in the Jinshi 1 well, 4029.21 m.

A microthermometric experiment was carried out on the fluid inclusions in the veins of carbonate reservoirs of the Lin 1 and Jinshi 1 wells. The results of temperature and freezing point measurements of primary brine inclusions in dolomite and quartz minerals of different periods in two wells show that the homogenization temperature and salinity of primary brine inclusions in dolomite I of the 4th member of the Dengying Formation in the Lin 1 well are 133.1–167.8 °C and 13.6–16.1%, respectively. The homogenization temperature of primary brine inclusions in the dolomite II ranges from 170.2 °C to 211.6 °C, and the salinity ranges from 16.7% to 20.7%. The homogenization temperature of primary saline inclusions in the quartz ranges from 121.2 °C to 164.2 °C, and the salinity ranges from 13.9% to 17.8%. The homogenization temperature and salinity of the primary brine inclusions in dolomite I and dolomite II reservoirs in the 2nd member of the Dengying Formation of the Jinshi 1 well are 112.9–136.7 °C, 9.7–11.9% and 131.5–159.7 °C, 10.7–12.7%, respectively. The homogenization temperature of primary brine inclusions in the dolomite III ranges from 153.3 °C to 174.9 °C, and the salinity ranges from 13.1% to 16.2% (Figure 8).

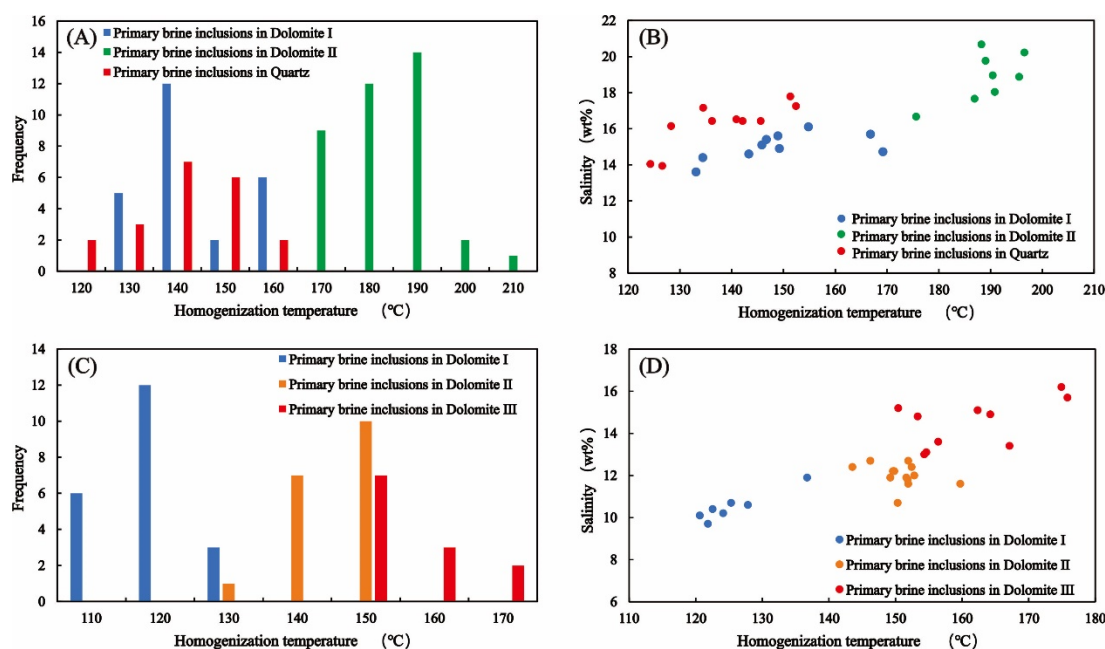


Figure 8. Histograms of the homogenization temperature distribution and the relationship between homogenization temperature and salinity of brine inclusions in dolomite and quartz of the Dengying Formation in the Lin 1 and Jinshi 1 wells: (A) Homogenization temperature distribution of primary brine inclusions in dolomite and quartz minerals in the 4th member of the Dengying Formation in the Lin 1 well; (B) the relationship between homogenization temperature and salinity of primary brine inclusions in dolomite and quartz minerals in the 4th member of the Dengying Formation in the Lin 1 well; (C) homogenization temperature distribution of primary brine inclusions in dolomite minerals in the 2nd member of the Dengying Formation in the Jinshi 1 well; (D) the relationship between homogenization temperature and salinity of primary brine inclusions in dolomite minerals in the 2nd member of the Dengying Formation in the Jinshi 1 well.

Through the analysis of petrographic characteristics of fluid inclusions in reservoir filling mineral particles and the identification of in situ Raman spectrum characteristic peak of fluid inclusions, the composition of fluid inclusions in mineral particles is accurately determined [54,55]. In the 4th member of the Dengying Formation in the Lin 1 well, pure methane gas inclusions (Figure 9A) and methane-bearing brine inclusions (Figure 9B) are developed in quartz minerals. The signal intensity of the methane characteristic peak is not obvious at 300 grating, but it is obvious at 1800 grating. The composition of methane-bearing brine inclusions is methane gas and a certain content of water (Figure 9B). A very small number of pure methane inclusions (Figure 9C) and a large number of methane-bearing brine inclusions are developed in dolomite minerals of the 2nd member of the Dengying Formation in the Jinshi 1 well. The composition of methane-bearing brine inclusions is methane gas and water with low signal intensity of methane characteristic peak (Figure 9D).

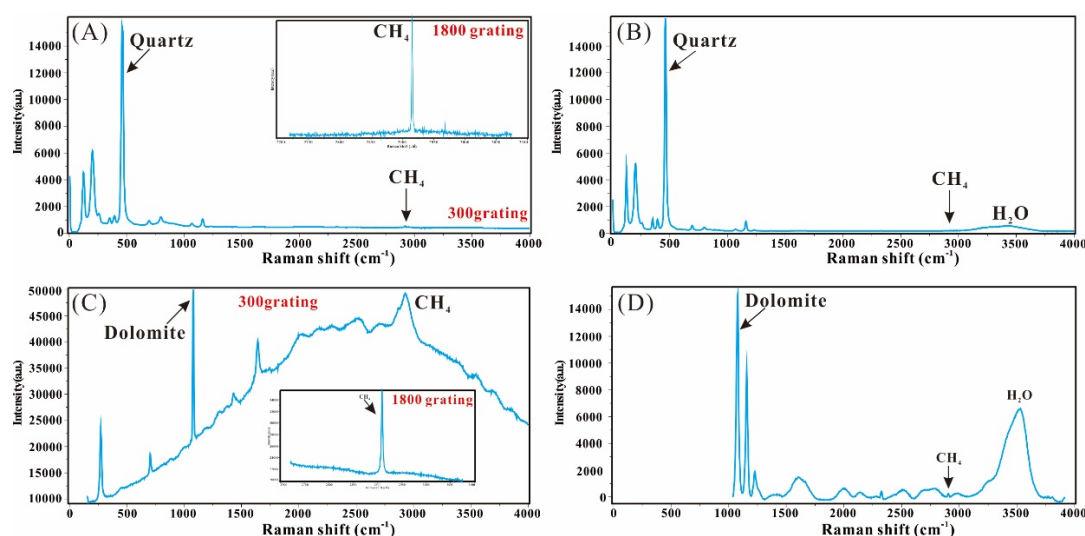


Figure 9. Laser Raman spectra of methane inclusions in the Dengying Formation of the Lin 1 and Jinshi 1 wells. Raman spectrum of pure CH₄ component collected using 300 gr.mm^{−1} grating in dolomite and quartz, CH₄ symmetric stretching band (ν_1) peak using 1800 gr.mm^{−1} grating. (A) pure methane gas inclusions in quartz minerals in the 4th member of the Dengying Formation in the Lin 1 well; (B) methane-bearing brine inclusions in quartz minerals in the 4th member of the Dengying Formation in the Lin 1 well; (C) pure methane inclusions in dolomite minerals in the 2nd member of the Dengying Formation in the Jinshi 1 well; (D) methane-bearing brine inclusions in dolomite minerals in the 2nd member of the Dengying Formation in the Jinshi 1 well.

4.5. BasinMod Simulates the Stage of Hydrocarbon Accumulation Evolution

The Cambrian Qiongzhusi Formation in the southeast and southwest of the Sichuan Basin is mainly composed of black and gray mudstone and shale, and the organic matter type is sapropelic kerogen. According to the actual situation in the southeast and southwest of the Sichuan Basin, the BasinMod1D software is used to reconstruct the hydrocarbon generation history of the Lin 1 and Jinshi 1 wells. The hydrocarbon generation evolution from the source rock of the Qiongzhusi Formation in the Lin 1 well (Figure 10A) can be divided into two geological time periods, the first period is 460–400 Ma, and the second period is 300–270 Ma. The first period was the early oil generation stage, accompanied by a small amount of natural gas generation; the second period was the main oil generation stage and gas generation stage, and the oil generation rate reaches a peak about 289 Ma. In the second period, the crude oil previously charged into the reservoir of the Dengying Formation was cracked in situ when the maturity reached and exceeded 2.0% R_o , resulting in a large amount of methane gas formation. The Cambrian Qiongzhusi Formation of the Jinshi 1 well in the southwest of the Sichuan Basin is mainly composed of black and gray mudstone and shale, and the organic matter type is mainly sapropelic kerogen. The hydrocarbon generation evolution of the source rock in the Jinshi 1 well (Figure 10B) can be divided into two geological time periods, the first period is 430–400 Ma, and the second period is 290–200 Ma. The first period was the early oil generation stage with less oil and gas generation, and the second period was a large oil generation and gas generation stage. The source rock of the Qiongzhusi Formation in the Jinshi 1 well generated a lot of oil at 290–230 Ma; the oil generation rate reached a maximum about 275 Ma and the gas generation rate reached the maximum at 280–270 Ma and continued until about 200 Ma.

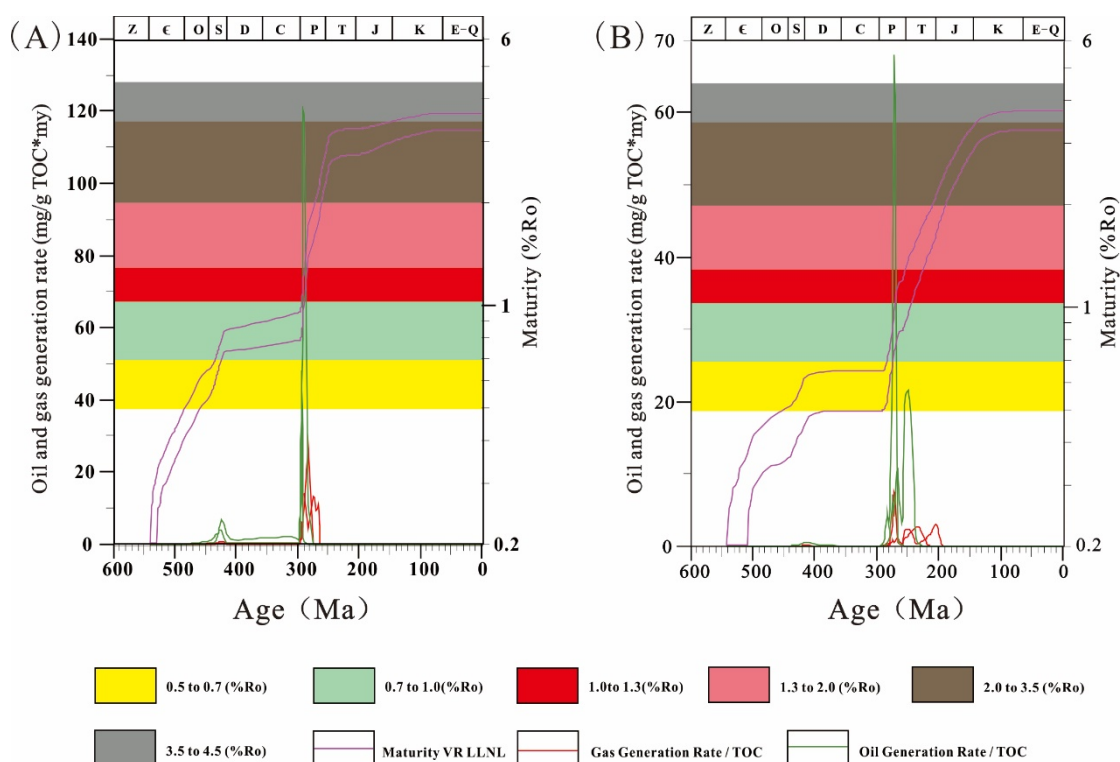


Figure 10. Maturity, hydrocarbon generation rate and hydrocarbon generation conversion history of source rocks in the Qiongzhusi Formation of the Lin 1 well (A) and the Jinshi 1 well (B).

5. Discussion

5.1. Rare Earth Elements Indicate the Characteristics of Dolomite Vein Fluids

The REE geochemistry characteristics of dolomite veins and dolomite filled in the Lin 1 and Jinshi 1 wells of the Dengying Formation represent the characteristics of the dolomite vein fluids, and, to some extent, reflect the source of dolomite vein fluids and the environment of dolomite vein formation [51,56–58]. The dolomite veins of the 4th member of the Dengying Formation in the Lin 1 well are characterized by a relative loss of LREE and relative enrichment of HREE, and they all show obvious negative Ce anomaly characteristics. It shows the characteristics of modern marine carbonate rocks [59,60]. The Y/Ho values also indicate a source of marine fluids [61]. The Dengying Formation is a marine carbonate sedimentary formation, and therefore, the dolomite veins are mainly derived from marine diagenetic fluids of the same layer. The REE distribution curves of dolomite II show positive Eu anomaly on the whole (Figure 6A), indicating that it is affected by hydrothermal activity to a certain extent [62–64]. The major positive Eu anomaly of dolomite II would be diagnostic of the mixing of marine diagenetic fluids with hydrothermal fluids [59]. The homogenization temperature of primary brine inclusions in dolomite II is 170.2–211.6 °C (Figure 8A), and the burial history shows that the time is in the Middle and Late Permian–Early Triassic period (Figure 11A), which is the active period of the Emei mantle plume activity (Figure 2) [65–67]. During this period, hydrothermal fluids entered dolomite in the carbonate reservoirs, which facilitated the exchange of cations between the rock and the hydrothermal fluids. The dolomite II vein-forming fluid influenced by the deep hydrothermal fluid caused by the activity of the Emei mantle plume.

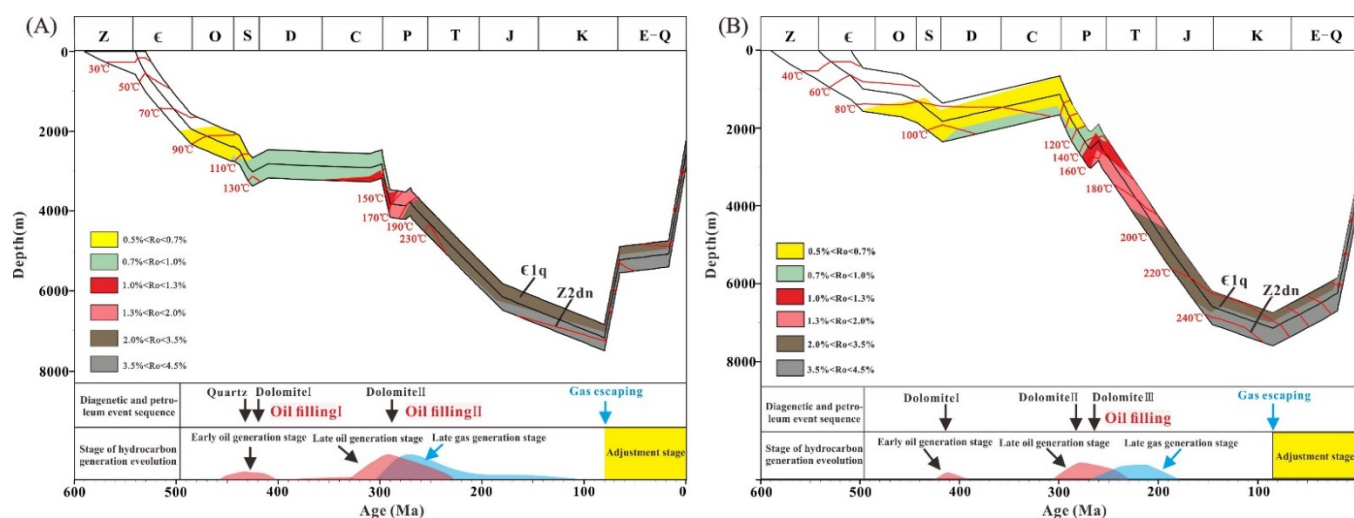


Figure 11. Burial history-thermal evolution map and paleo-fluid evolution sequence of the Dengying Formation in the Lin 1 well (A) and the Jinshi 1 well (B).

The rare earth elements in the dolomite veins of the 2nd member of the Dengying Formation in the Jinshi 1 well in the southwest of the Sichuan Basin show negative Ce anomaly and high Y/Ho values, indicating the characteristics of marine fluids. The results indicate that the dolomite vein-forming fluids are mainly derived from marine diagenetic fluids in the formation, just as in the Lin 1 well. Dolomite II and dolomite III show Eu positive anomaly characteristics, and the source of the vein-forming fluid is a mixture of marine diagenetic fluid and hydrothermal fluid (Figure 6B). The homogenization temperatures of primary brine inclusions in the minerals of the dolomite II and dolomite III in the Jinshi 1 well range from 131.5 °C to 159.7 °C and 153.3 °C to 174.9 °C, respectively, indicating that the age is in the Middle Permian–Triassic period (Figure 11B), which is also the active period of the Emei mantle plume activity. Therefore, the influence of hydrothermal activity on dolomite comes from the deep hydrothermal activity caused by the Emei mantle plume activity (Figure 2).

5.2. Carbon, Oxygen, and Strontium Isotopes Indicate the Characteristics of Dolomite Vein Fluids

The isotopic geochemistry characteristics of dolomite veins can also indicate the source of the fluid [68–70]. The results show that the dolomite veins and mineral fluids in the Dengying Formation of the Lin 1 and Jinshi 1 wells are derived from carbonate diagenetic fluids of sedimentary origin (Figure 12). The $\delta^{18}\text{O}_{\text{PDB}}$ values of dolomite filled in the 4th member of the Dengying Formation in the Lin 1 well range from -12.81‰ to -11.75‰ , and the surrounding rock is -10.21‰ (Table 2), both of which are highly negative values, indicating that the dolomite may be formed from diagenetic fluid in a diagenetic environment. The $\delta^{13}\text{C}_{\text{PDB}}$ ranges from 0.42‰ to 2.46‰, and the surrounding rock is 3.06‰. The $\delta^{13}\text{C}_{\text{PDB}}$ values of most marine carbonate rocks are between 4‰ and -4‰ , indicating that marine carbonate is the most important carbon source of dolomite filled in the 4th member of the Dengying Formation in the Lin 1 well [70] and the carbon in dolomite veins may mainly come from surrounding rock. The $\delta^{18}\text{O}_{\text{PDB}}$ values of dolomite filled in the 2nd member of the Dengying Formation in the Jinshi 1 well range from -10.34‰ to -9.63‰ , and the surrounding rock is -5.56‰ (Table 2), both of which are high negative values on the whole. The $\delta^{13}\text{C}_{\text{PDB}}$ ranges from 2.66‰ to 2.82‰, and the surrounding rock is 3.70‰, which are similar to the characteristics of the Lin 1 well. It indicates that the carbon in dolomite veins in the 2nd member of the Dengying Formation of the Jinshi 1 well is mainly derived from surrounding rock. The $\delta^{13}\text{C}_{\text{PDB}}$ and $\delta^{18}\text{O}_{\text{PDB}}$ values of the 2nd member of the Dengying Formation in the Jinshi 1 well are higher than

those of the 4th member of the Dengying Formation in the Lin 1 well, probably caused by isotopes fractionation in elevated temperatures.

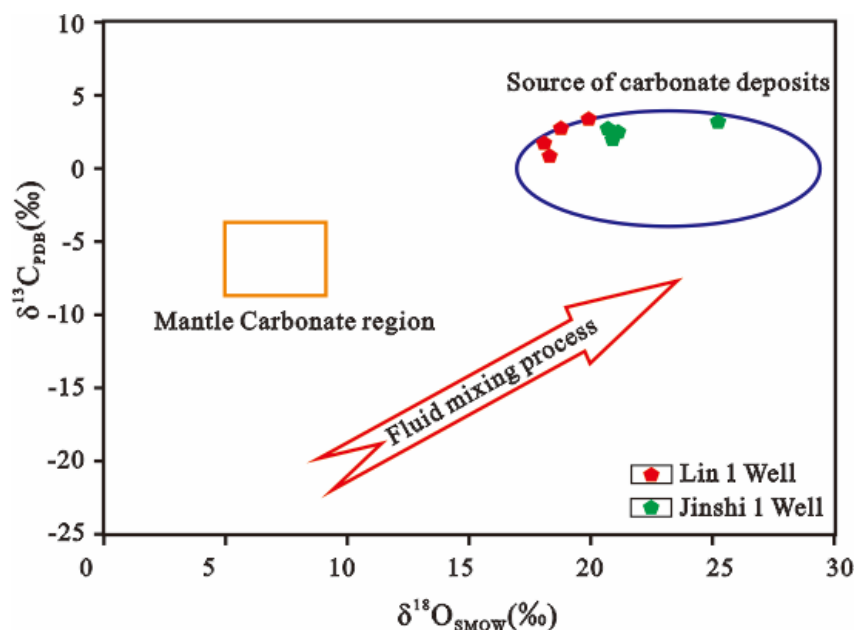


Figure 12. The $\delta^{13}\text{C}$ and $\delta^{18}\text{O}$ discrete diagram of filling minerals in the 4th member of the Dengying Formation reservoir in the Lin 1 well and the 2nd member of the Dengying Formation reservoir in the Jinshi 1 well.

The residence time of strontium element in seawater is much longer than the mixing time of seawater, therefore, the isotopic composition of marine strontium element is uniform at any time, worldwide. The $^{87}\text{Sr}/^{86}\text{Sr}$ value of dolomite can basically represent the $^{87}\text{Sr}/^{86}\text{Sr}$ ratio of the original fluid during mineral crystallization and precipitation [27,71]. The $^{87}\text{Sr}/^{86}\text{Sr}$ value of dolomite filled in the 4th member of the Dengying Formation in the Lin 1 well ranges from 0.711359 to 0.714824, and the $^{87}\text{Sr}/^{86}\text{Sr}$ value of surrounding rock is 0.709935 (Table 2), which is significantly higher than the $^{87}\text{Sr}/^{86}\text{Sr}$ value of sea water in the Dengying Formation of the same period, 0.7083. It indicates that the vein forming fluid was influenced by strontium-rich fluid [72], which may be related to the denudation of the 4th member of the Dengying Formation by the Tongwan movement [73,74] in the Sinian period (Figure 2). The Tongwan movement caused the strata of the 4th member of the Dengying Formation to be uplifted to the surface and subjected eluviation of atmospheric fresh water which was the rich strontium of crustal origin fluid. The strontium isotope ratio of the crust derived from the chemical weathering of the old silicon-aluminum rocks in the continental crust into the ocean is relatively high, and the average ratio is estimated to be 0.720 ± 0.005 [75]. Therefore, the strontium isotope value of the dolomite filled in the 4th member of the Dengying Formation in the Lin 1 well is relatively high.

5.3. Formation Time of Dolomite Veins and Minerals

The homogenization temperature of brine inclusion captured at the same time with methane inclusion represents the capture temperature of methane inclusion at that time, and the capture temperature of primary brine inclusion captured by mineral growth represents the temperature of mineral formation [76,77]. The formation time of veins and minerals can be determined by temperature projection in the burial history. The homogenization temperature may increase as fluid inclusions trapped in minerals undergo deformation, fluid leakage, and rebalancing. As for fluid inclusions in carbonate minerals, they are more likely to be modified later, and therefore, the minimum homogenization temperature of primary brine inclusions in dolomite and quartz is selected to represent the formation temperature of veins to determine the formation time of minerals and veins [78–80]. The

results show that the formation time of dolomite I in the 4th member of the Dengying Formation in the Lin 1 well is about 421 Ma, the formation time of dolomite II is about 288 Ma, the formation time of quartz is about 432 Ma, and the capture time of secondary methane inclusions in quartz is about 20 Ma (Figure 11A). The formation times of dolomite I, dolomite II, and dolomite III in the 2nd member of the Dengying Formation in the Jinshi 1 well is about 425 Ma, 283 Ma, and 262 Ma, respectively, and the capture time of methane-bearing brine inclusions in the dolomite III is about 19 Ma (Figure 11B).

5.4. Multistage Fluid and Process of Hydrocarbon Accumulation

Based on the study of the hydrocarbon accumulation process of the lower Paleozoic in the southeast of the Sichuan Basin, the hydrocarbon generation evolution stage of the Cambrian source rocks and hydrocarbon charging time of the Dengying Formation in the southeast of the Sichuan Basin are determined. The 4th member of the Dengying formation reservoir in the southeast of the Sichuan Basin started oil charging about 460–400 Ma, and then, denudation resulted in hydrocarbon generation stagnation of source rocks and destruction of paleo reservoirs; about 300–270 Ma, the Cambrian source rocks entered the late oil generation stage, followed by the second oil charging stage; about 270 Ma, the reservoir entered the stage of oil cracking and generating dry gas and asphalt; and since the late Yanshan period, the strata were uplifted and denuded violently, forming faults connected to the surface [12,17], causing a large amount of natural gas to escape, and destroying the gas reservoir. The fluid evolution sequence of the 4th member of the Dengying Formation within the Lin 1 well in the southeast of the Sichuan Basin is as follows: quartz (~432 Ma) → dolomite I (~421 Ma) → oil filling I (460–400 Ma) → dolomite II (~288 Ma) → oil filling II (300–270 Ma) → gas escaping (~75 Ma) (Figure 11A). The recovery pressure coefficient of secondary methane inclusion captured from quartz of the 4th member of the Dengying Formation in the Lin 1 well is 0.85–1.06, which is a normal pressure and poor preservation condition. The homogenization temperature of brine inclusions associated with the secondary methane inclusions shows that the capture time of methane inclusions is about 20 Ma (Figure 11A). After the Himalayan uplift tectonism, natural gas was lost and the formation pressure and pressure coefficient decreased, and about 60 Ma, the Dengying Formation reservoir returned to a normal pressure state [81]. The methane inclusions captured by the quartz minerals in the 4th member of the Dengying Formation in the Lin 1 well are secondary methane inclusions, which were captured when the gas reservoir was destroyed, so the formation pressure is a normal pressure.

The reservoir of the 2nd member of the Dengying Formation in the southwest of the Sichuan Basin began the first phase of oil charging about 430–400 Ma, and the subsequent denudation caused the stagnation of hydrocarbon generation in the source rocks and destroyed paleo-oil reservoirs at the same time; about 290 Ma, the Cambrian source rock entered the late oil generation stage, followed by the second stage of oil charging in the reservoir; about 290–230 Ma, the reservoir entered the stage of crude oil cracking into gas, generating dry gas and asphalt. During the Himalayan period, the axis of the Leshan-Longnvsi paleo uplift migrated to the Weiyuan structure, while the strata of the Weiyuan structure uplifted sharply, and the overlying strata suffered severe denudation and formed the largest anticline in the Sichuan Basin, the Weiyuan anticline [82–84]. At this time, the Jinshi structure became a secondary anticline in the southwest slope belt of the Weiyuan anticline. The reservoir fluid evolution sequence of the 2nd member of the Dengying Formation in the Jinshi 1 well in the southwest of the Sichuan Basin is as follows: dolomite I (~425 Ma) → oil filling I (430–400 Ma) → dolomite II (~283 Ma) → oil filling II (290–230 Ma) → dolomite III (~262 Ma) → gas escaping (~85 Ma) (Figure 11B). The methane inclusions and brine inclusions in the same fluid inclusion combination on the surface of dolomite mineral particles are captured at the same time, and the capture time of methane-bearing brine inclusions is about 19 Ma which is the period of stratigraphic uplift and denudation (Figure 11B). The methane laser Raman peak displacements of methane-bearing brine inclusions that are developed in the dolomite of the Jinshi 1 well

are distributed in the range of 2913.44~2914.49 cm⁻¹. The paleo-pressure recovery shows that it is a normal pressure, indicating that the natural gas is captured in the process of gas reservoir adjustment and escape. This is mainly due to the change in the high point of the Jinshi structure. With the formation of the Wei yuan uplift, the Jinshi structure evolves from a higher position to a low structure position, and the natural gas migrates to the Wei yuan structure [85,86], during which a small amount of natural gas is captured by dolomite under normal pressure.

6. Conclusions

- (1) The results of vein petrography, cathodoluminescence, and in situ microanalysis of elements from the studied samples show that two stages of dolomite and one stage of quartz are developed in the 4th member of the Dengying Formation in the southeast of the Sichuan Basin, and three stages of dolomite are developed in the 2nd member of the Dengying Formation in the southwest of the Sichuan Basin.
- (2) Rare earth elements and carbon, oxygen, and strontium isotopes with the studied samples indicate that the source of dolomite vein-forming fluids in the two development stages of the 4th member of the Dengying Formation in the southeast of the Sichuan Basin were marine reservoir diagenetic fluids. The dolomite II REE distribution curves show obvious positive Eu anomaly on the whole, indicating that it was affected by a certain degree of hydrothermal activity, which may have been caused by the deep hydrothermal activity of the Emei mantle plume. The dolomite vein-forming fluids of the three development stages of the 2nd member of the Dengying Formation in the southwest of the Sichuan Basin were the sources of marine reservoir diagenetic fluid. The REE distribution curves of dolomite II and dolomite III show a certain degree of Eu positive anomaly, indicating that they were all affected by hydrothermal activity. The influence of hydrothermal activity on dolomite came from the deep hydrothermal activity caused by the Emei mantle plume activity.
- (3) The carbon and oxygen isotope values of the dolomite vein samples of the 4th member of the Dengying Formation in the southeast of the Sichuan Basin are smaller than those of the 2nd member of the Dengying Formation in the southwest of the Sichuan Basin, showing a negative deviation. The vein forming fluid of the 4th member of the Dengying Formation in the southeast of the Sichuan Basin is affected by strontium-rich fluid (crust source strontium), while the 2nd member of the Dengying Formation in the southwest of the Sichuan Basin may not be affected by obvious strontium-rich fluid.
- (4) The formation time of dolomite I in the 4th member of the Dengying Formation in the southeast of the Sichuan Basin was about 421 Ma, the formation time of dolomite II was about 288 Ma, the formation time of quartz was about 432 Ma, and the capture time of secondary methane inclusions in quartz was about 20 Ma. The formation times of dolomite I, dolomite II, and dolomite III in the 2nd member of the Dengying Formation in the southwest of the Sichuan Basin were about 425 Ma, 283 Ma, and 262 Ma, respectively, and the capture time of methane-bearing brine inclusions in the dolomite III was about 19 Ma.
- (5) The fluid activity and hydrocarbon accumulation evolution sequence in the southeast and southwest of the Sichuan Basin are determined comprehensively. The sequence of the 4th member of the Dengying Formation in the southeast of the Sichuan Basin is as follows: quartz (~432 Ma) → dolomite I (~421 Ma) → oil filling I (460–400 Ma) → dolomite II (~288 Ma) → oil filling II (300–270 Ma) → gas escaping (~75 Ma). The sequence of the 2nd member of the Dengying Formation in the southwest of the Sichuan Basin is as follows: dolomite I (~425 Ma) → oil filling I (430–400 Ma) → dolomite II (~283 Ma) → oil filling II (290–230 Ma) → dolomite III (~262 Ma) → gas escaping (~85 Ma).

Author Contributions: Conceptualization, J.L. and S.H.; methodology, F.W. and S.H.; formal analysis, J.L., Y.Z. and T.L.; resources, Z.H., D.Z. and Z.S.; data curation, J.L., F.W., S.H.; writing—original draft

preparation, J.L.; writing—review and editing, J.L., F.W., S.H. and Y.H.; project administration, Z.H., D.Z. and Z.S. All authors have read and agreed to the published version of the manuscript.

Funding: This research was funded by the scientific research project of SINOPEC (No. P19022-3), the National Natural Science Foundation Project of China (No. U20B6001), and the National Natural Science Foundation of China (No. 41830431).

Data Availability Statement: The data used to support the findings of this study are included within the article.

Acknowledgments: The study was financially supported by the authors acknowledge funding from the scientific research project of SINOPEC (No. P19022-3), the National Natural Science Foundation Project of China (No. U20B6001), and the National Natural Science Foundation of China (No. 41830431). We are very grateful to the Petroleum Exploration and Production Research Institute of SINOPEC, for their kind help and support to complete this study and the permission to publish the results.

Conflicts of Interest: The authors declare no conflict of interest.

References

1. He, Z.L.; Jin, X.H.; Wo, Y.J.; Li, H.L.; Bai, Z.R.; Jiao, C.L.; Zhang, Z.P. Hydrocarbon accumulation characteristics and exploration domains of ultra-deep marine carbonates in China. *China Pet. Explor.* **2016**, *21*, 3–14. (In Chinese with English Abstract)
2. Ma, Y.S.; Cai, X.Y.; Zhao, P.R. The research status and advances in porosity evolution and diagenesis of deep carbonate reservoir. *Earth Sci. Front.* **2011**, *18*, 181–192.
3. Heydari, E. Porosity loss, fluid flow, and mass transfer in limestone reservoirs: Application to the Upper Jurassic Smackover Formation, Mississippi. *AAPG Bull.* **2000**, *84*, 100–118.
4. Jin, Z.J. Formation and accumulation of oil and gas in marine carbonate strata in Chinese sedimentary basins. *Sci. China Earth Sci.* **2011**, *41*, 910–926.
5. Zhu, G.Y.; Zhang, S.C. Hydrocarbon accumulation conditions and exploration potential of deep reservoirs in China. *Acta Pet. Sin.* **2009**, *30*, 793–802.
6. Zou, C.N.; Du, J.H.; Xu, C.C.; Wang, Z.C.; Zhang, B.M.; Wei, G.Q.; Wang, T.S.; Yao, G.S.; Deng, S.H.; Liu, J.J.; et al. Formation, distribution, resource potential and discovery of the Sinian-Cambrian giant gas field, Sichuan Basin, SW China. *Pet. Explor. Dev.* **2014**, *41*, 278–293. [[CrossRef](#)]
7. Du, J.H.; Zou, C.N.; Xu, C.C.; He, H.Q.; Shen, P.; Yang, Y.M.; Li, Y.L.; Wei, G.Q.; Wang, Z.C.; Yang, Y. Theoretical and technical innovations in strategic discovery of a giant gas field in Cambrian Longwangmiao Formation of central Sichuan paleo-uplift, Sichuan Basin. *Pet. Explor. Dev.* **2014**, *41*, 294–305. [[CrossRef](#)]
8. Wei, G.Q.; Du, J.H.; Xu, C.C.; Zou, C.N.; Yang, W.; Shen, P.; Xie, Z.Y.; Zhang, J. Characteristics and accumulation modes of large gas reservoirs in Sinian-Cambrian of Gaoshiti-Moxi region, Sichuan Basin. *Acta Pet. Sin.* **2015**, *36*, 1–12. [[CrossRef](#)]
9. Wang, Z.C.; Wang, T.S.; Wen, L.; Jiang, H.; Zhang, B.M. Basic geological characteristics and accumulation conditions of Anyue giant gas field, Sichuan Basin. *China Offshore Oil Gas* **2016**, *28*, 45–52. (In Chinese with English Abstract).
10. Fan, T.Y.; Jiang, L.; Nie, Q.; Zhao, W.T.; Wu, Y.; Geng, C.; Zou, X.; Li, T. Evaluation on development potential in the Lower Cambrian Longwangmiao Formation, Gaoshiti block, Anyue gasfield, Sichuan Basin. *Nat. Gas Explor. Dev.* **2021**, *44*, 44–55. (In Chinese with English Abstract)
11. Li, S.; Zhou, Y.; Xiao, K.; Wo, Y. Characteristics of Silurian destroyed oil reservoir in Houtan section of Xishui area in southeastern margin of Sichuan Basin. *Acta Pet. Sin.* **2009**, *30*, 849–855.
12. Sun, W.; Liu, S.G.; Wang, G.Z.; Xu, G.S.; Yong, Z.Q.; Huang, W.M. Petroleum formed condition and process research for Sinian to Low Paleozoic at Dingshan structure in southeast of Sichuan Basin. *Geol. Sci. Technol. Inf.* **2010**, *29*, 49–55. (In Chinese with English Abstract)
13. Wei, G.Q.; Shen, P.; Yang, W.; Zhang, J.; Jiao, G.H.; Xie, W.R.; Xie, Z.Y. Formation conditions and exploration prospects of Sinian large gas fields, Sichuan Basin. *Pet. Explor. Dev.* **2013**, *40*, 129–138. [[CrossRef](#)]
14. Chang, Y.Q.; Sun, W.; Li, Z.Q.; Ye, Y.H.; Jiao, K.; Yuan, Y.; Tian, M.N. Oil and gas exploration prospects of the deep buried Dengying Formation in the southeastern Sichuan Basin, China. *J. Chengdu Univ. Technol. Sci. Technol. Ed.* **2019**, *46*, 142–152. (In Chinese with English Abstract)
15. Liu, S.G.; Ma, Y.S.; Huang, W.M.; Cai, X.Y.; Zhang, C.J.; Wang, G.Z.; Xu, G.S.; Yong, Z.Q.; Pan, C.L. Densification process of upper Sinian Dengying Formation, Sichuan Basin. *Nat. Gas Geosci.* **2007**, *18*, 485–496.
16. Zhou, Z.; Wang, X.Z.; Xie, L.; Mo, J.; Zhang, J. Reservoir features and physical influences of the Sinian Dengying Formation (Sinian) in central Sichuan, China. *Nat. Gas Geosci.* **2014**, *25*, 701–708.
17. Shi, Z.J.; Peng, J.; Wang, Y. Reservoir features and controlling factors of Dengying Formation in southeast Sichuan, China. *J. Chengdu Univ. Technol. Sci. Technol. Ed.* **2010**, *37*, 1–8. (In Chinese with English Abstract)
18. Zhu, D.Y.; Zhang, D.W.; Liu, Q.Y.; He, Z.L.; Li, S.J.; Zhang, R.Q. Dynamic development process and mechanism of dolomite reservoir under multi-fluid alterations. *Nat. Gas Geosci.* **2015**, *26*, 2053–2062.

19. Yang, P.; Xie, Y.; Wang, Z.J.; Li, Q.Y.; Liu, J.H.; Zhang, D.; Yang, Z.; Yin, F. Fluid activity and hydrocarbon accumulation period of Sinian Dengying Formation in Northern Guizhou, South China. *Pet. Explor. Dev.* **2014**, *41*, 313–335. [[CrossRef](#)]
20. Wei, G.Q.; Yang, W.; Du, J.H.; Xu, C.C.; Zou, C.N.; Xie, W.R.; Wu, S.J.; Zeng, F.Y. Tectonic features of Gaoshiti-Moxi paleo-uplift and its controls on the formation of a giant gas field, Sichuan Basin, SW China. *Pet. Explor. Dev.* **2015**, *42*, 257–265. [[CrossRef](#)]
21. Ma, W.X.; Liu, S.G.; Huang, W.M.; Zhang, C.J.; Xu, G.S.; Yuan, H.F. Characteristics of Silurian Paleo-oil reservoirs and their significance for petroleum exploration on the southeast margin of Sichuan Basin. *Oil Gas Geol.* **2012**, *33*, 432–441.
22. Wang, G.Z.; Liu, S.G.; Liu, W.; Fan, L.; Yuan, H.F. Process of hydrocarbon accumulation of Sinian Dengying Formation in Gaoshiti structure, Central Sichuan, China. *J. Chengdu Univ. Technol. Sci. Technol. Ed.* **2014**, *41*, 684–693. (In Chinese with English Abstract)
23. Huang, W.M.; Liu, S.G.; Xu, G.S.; Wang, G.Z.; Ma, W.X.; Zhang, C.J.; Song, G.Y. Characteristics of paleo oil pools from Sinian to Lower Paleozoic in southeastern margin of Sichuan Basin. *Geol. Rev.* **2011**, *57*, 285–299. (In Chinese with English Abstract)
24. Liu, S.G.; Qin, C.; Sun, W.; Wang, G.Z.; Xu, G.S.; Yuan, H.F.; Zhang, C.J.; Zhang, C.J. The coupling formation process of four centers of hydrocarbon in Sinian Dengying Formation of Sichuan Basin. *Acta Petrol. Sin.* **2012**, *28*, 879–888.
25. Jiang, H.; Wang, Z.C.; Du, H.Y.; Zhang, C.M.; Wang, R.J.; Zou, N.N.; Wang, T.S.; Gu, Z.D.; Li, Y.X. Tectonic evolution of the Leshan-Longnvsi paleo-uplift and reservoir formation of Neoproterozoic Sinian gas. *Nat. Gas Geosci.* **2014**, *25*, 192–200.
26. Sun, W.; Liu, S.G.; Song, J.M.; Deng, B.; Wang, G.Z.; Wu, J.; Jiao, K.; Li, J.X.; Ye, Y.H.; Li, Z.W.; et al. The formation process and characteristics of ancient and deep carbonate petroleum reservoirs in superimposed basins: A case study of Sinian (Ediacaran) Dengying Formation in the Sichuan superimposed basin, China. *J. Chengdu Univ. Technol. Sci. Technol. Ed.* **2017**, *44*, 257–285. (In Chinese with English Abstract)
27. Wang, G.Z.; Liu, S.G. Paleo-fluid geochemical evaluation of hydrocarbon preservation in marine carbonate rock areas: Taking lower association in central Sichuan Basin as an example. *J. Chengdu Univ. Technol. Sci. Technol. Ed.* **2009**, *36*, 631–644. (In Chinese with English Abstract)
28. Shi, Z.J.; Wang, Y.; Tian, Y.M.; Wang, C.C. Cementation and diagenetic fluid of algal dolomites in the Sinian Dengying Formation in southeastern Sichuan Basin. *Sci. China Earth Sci.* **2013**, *56*, 192–202. [[CrossRef](#)]
29. Feng, M.Y.; Qiang, Z.T.; Shen, P.; Zhang, J.; Tao, Y.Z.; Xia, M.L. Evidences for hydrothermal dolomite of Sinian Dengying Formation in Gaoshiti-Moxi area, Sichuan Basin. *Acta Pet. Sin.* **2016**, *37*, 587–598.
30. Luo, B.; Yang, Y.M.; Luo, W.J.; Wen, L.; Wang, W.Z.; Chen, K. Controlling factors and distribution of reservoir development in Dengying Formation of paleo-uplift in central Sichuan Basin. *Acta Pet. Sin.* **2015**, *36*, 416–426.
31. Eichhubl, P.; Boles, J.R. Focused fluid flow along faults in the Monterey Formation, coastal California. *Geol. Soc. Am. Bull.* **2000**, *112*, 1667–1679. [[CrossRef](#)]
32. Ye, J.R.; Yang, X.H. Thermal fluid flow in sedimentary basins and its significance to pool-forming dynamics. *Acta Sedimentol. Sin.* **2001**, *19*, 214–218. (In Chinese with English Abstract)
33. Williams, R.T.; Goodwin, L.B.; Mozley, P.S.; Beard, B.L.; Johnson, C.M. Tectonic controls on fault zone flow pathways in the Rio Grande rift, New Mexico, USA. *Geology* **2015**, *43*, 723–726. [[CrossRef](#)]
34. Gui, L.L.; Zhao, M.J.; Liu, K.Y.; Luo, M.; Meng, Q.Y.; Yuan, L.; Hao, J.Q. Reservoir fluid evolution and hydrocarbon charge history of the Gasi E13 Oilfield, southwestern Qaidam Basin. *Nat. Gas Geosci.* **2016**, *27*, 289–297.
35. Luo, T.; Guo, X.W.; Shu, Z.G.; Bao, H.Y.; He, S.; Qin, Z.J.; Xiao, Z.H. Fluid source and formation time of fracture veins of Wufeng Formation and Longmaxi Formation in the south of Jiaoshiba area, Sichuan Basin. *Acta Pet. Sin.* **2021**, *42*, 611–622.
36. Wei, G.Q.; Yang, W.; Xie, W.R.; Xie, Z.Y.; Zeng, F.Y.; Mo, W.L.; Shen, J.H.; Jin, H. Formation conditions, accumulation models and exploration direction of large gas fields in Sinian-Cambrine, Sichuan Basin. *Nat. Gas Geosci.* **2015**, *26*, 785–795.
37. Liu, S.G.; Sun, W.; Li, Z.W.; Deng, B.; Zhong, Y.; Song, J.M.; Ran, B.; Luo, Z.L.; Han, K.Y.; Jiang, L.; et al. Distribution characteristics of marine carbonate reservoirs and their tectonic controlling factors across the Sichuan superimposed basin. *Lithol. Res.* **2016**, *28*, 1–17. (In Chinese with English Abstract)
38. Sun, Z.M.; Zhang, R.Q.; Sun, W.; Hao, Y.Q.; Bian, C.R. Petroleum exploration domains and favorable directions of the lower marine assemblage in Eastern Sichuan Basin. *Geoscience* **2021**, *35*, 798–806. (In Chinese with English Abstract)
39. Qin, Z.P.; Liu, S.G.; Deng, B.; Li, Z.W.; Sun, W. Multiphase structural features and evolution of Southeast Sichuan tectonic belt in China. *J. Chengdu Univ. Technol. Sci. Technol. Ed.* **2013**, *40*, 703–711. (In Chinese with English Abstract)
40. Zhang, G.C. Analysis on carbonate hydrocarbon exploration potential from Sinian to Silurian in southeast of Sichuan. *S. China Oil Gas* **2003**, *16*, 15–18. (In Chinese with English Abstract)
41. Liu, R.B.; Tian, J.C.; Wei, Z.H.; Zhang, M.W.; Zhong, S.Q.; Zhang, G.H.; Wang, B. Comprehensive research of effective hydrocarbon source rock of lower strata from Sinian to Silurian system in southeast area of Sichuan Province. *Nat. Gas Geosci.* **2006**, *17*, 824–827.
42. Zhang, G.Y.; Zhao, W.Z.; Zou, C.N.; Li, W.; Fang, X. Petroleum geological conditions and exploration potential in middle and lower combinations of onshore superimposed basins in China. *Earth Sci. Front.* **2008**, *15*, 120–126.
43. Wang, X.Z.; Mu, S.G.; Fang, S.X.; Huang, J.X.; Hou, F.H. Evolution of porosity in the process of Sinian dolostone diagenesis in Southwest Sichuan. *Acta Sedimentol. Sin.* **2000**, *18*, 549–554. (In Chinese with English Abstract)
44. Shi, Z.J.; Liang, P.; Wang, Y.; Hu, X.Q.; Tian, Y.M.; Wang, C.C. Geochemical characteristics and genesis of grapestone in Sinian Dengying Formation in south-eastern Sichuan Basin. *Acta Petrol. Sin.* **2011**, *27*, 2263–2271.
45. Huang, H.; Chen, X.D.; Hu, H.W. The division and analysis of the favorable reservoir depositional facies of the Dengying Formation Upper-Sinian in southeastern Sichuan Basin. *Petrochem. Ind. Appl.* **2012**, *31*, 49–53. (In Chinese with English Abstract)

46. Zhou, J.G.; Zhang, J.Y.; Deng, H.Y. Lithofacies paleogeography and sedimentary model of Sinian Dengying Fm in the Sichuan Basin. *Nat. Gas Ind.* **2017**, *37*, 24–31. [\[CrossRef\]](#)
47. Duan, J.B.; Mei, Q.H.; Li, B.S.; Liang, Z.R. Sinian-early Cambrian tectonic-sedimentary evolution in Sichuan Basin. *Earth Sci.* **2019**, *44*, 738–755.
48. Coryell, C.D.; Chase, J.W.; Winchester, J.W. A procedure for geochemical interpretation of terrestrial rare-earth abundance patterns. *J. Geophys. Res.* **1963**, *68*, 559–566. [\[CrossRef\]](#)
49. Piper, D.Z. Rare earth elements in the sedimentary cycle: A summary. *Chem. Geol.* **1974**, *14*, 285–304. [\[CrossRef\]](#)
50. Hecht, L.; Freiburger, R.; Gilg, H.A.; Grundmann, G.; Kostitsyn, Y.A. Rare earth element and isotope (C, O, Sr) characteristics of hydrothermal carbonates: Genetic implications for dolomite-hosted talc mineralization at Gopfersgrun (Fichtelgebirge, Germany). *Chem. Geol.* **1999**, *155*, 115–130. [\[CrossRef\]](#)
51. Zhao, Y.Y.; Li, S.Z.; Li, D.; Guo, L.L.; Dai, L.M.; Tao, J.L. Rare earth element geochemistry of carbonate and its paleoenvironmental implications. *Geotecton. Metallog.* **2019**, *43*, 141–167. (In Chinese with English Abstract)
52. Wu, Z.R.; He, S.; He, X.P.; Zhai, G.Y.; Huang, Y.H.; Zhao, W.; Han, Y.J.; Yang, R. Characteristics of fluid inclusions in fracture calcite veins and implications of upper Permian Dalong Formation shale at the Lianyuan Depression. *Geol. Sci. Technol. Inf.* **2019**, *38*, 70–81.
53. Liu, L.; He, S.; Zhai, G.Y.; Chen, K.; Liu, Z.X.; Wang, Y.; Han, Y.J.; Dong, T. Diagenetic environment evolution of fracture veins of shale core in second member of Niutitang Formation in southern limb of Huangling Anticline and its connection with shale gas preservation. *Earth Sci.* **2019**, *44*, 3583–3597.
54. Kawakami, Y.; Yamamoto, J.; Kagi, H. Micro-Raman densimeter for CO₂ inclusions in mantle-derived minerals. *Appl. Spectrosc.* **2003**, *57*, 1333–1339. [\[CrossRef\]](#)
55. Dubessy, J.; Buschaert, S.; Lamb, W.; Pironon, J.; Thiéry, R. Methane-bearing aqueous fluid inclusions: Raman analysis, thermodynamic modelling and application to petroleum basins. *Chem. Geol.* **2001**, *173*, 193–205. [\[CrossRef\]](#)
56. Haskin, L.A.; Haskin, M.A.; Frey, F.A.; Wideman, T.R. Relative and absolute terrestrial abundances of the rare earths. *Orig. Distrib. Elem.* **1968**, 889–912.
57. Nothdurft, L.D.; Webb, G.E.; Kamber, B.S. Rare earth element geochemistry of Late Devonian reefal carbonates, Canning Basin, Western Australia: Confirmation of a seawater REE proxy in ancient limestones. *Geochim. Cosmochim. Acta* **2004**, *68*, 263–283. [\[CrossRef\]](#)
58. Alexander, B.W.; Bau, M.; Andersson, P.; Dulski, P. Continently-derived solutes in shallow Archean seawater: Rare earth element and Nd isotope evidence in iron formation from the 2.9 Ga Pongola Supergroup, South Africa. *Geochim. Cosmochim. Acta* **2008**, *72*, 378–394. [\[CrossRef\]](#)
59. Tostvein, R.; Shields, G.A.; Tarbuck, G.M.; He, T.; Clarkson, M.O.; Wood, R.A. Effective use of cerium anomalies as a redox proxy in carbonate-dominated marine settings. *Chem. Geol.* **2016**, *438*, 146–162. [\[CrossRef\]](#)
60. Zhao, Y.; Wei, W.; Li, S.; Yang, T.; Zhang, R.; Somerville, I.; Santosh, M.; Wei, H.; Wu, H.; Yang, J.; et al. Rare earth element geochemistry of carbonates as a proxy for deep-time environmental reconstruction. *Palaeogeogr. Palaeoclimatol. Palaeoecol.* **2021**, *574*, 110443. [\[CrossRef\]](#)
61. Bau, M.; Dulski, P. Comparing yttrium and rare earths in hydrothermal fluids from the Mid-Atlantic Ridge: Implications for Y and REE behaviour during near-vent mixing and for the Y/Ho ratio of Proterozoic seawater. *Chem. Geol.* **1999**, *155*, 77–90. [\[CrossRef\]](#)
62. Mitra, A.; Elderfield, H.; Greaves, M.J. Rare earth elements in submarine hydrothermal fluids and plumes from the Mid-Atlantic Ridge. *Mar. Chem.* **1994**, *46*, 217–235. [\[CrossRef\]](#)
63. James, R.H.; Elderfield, H. Chemistry of ore-forming fluids and mineral formation rates in an active hydrothermal sulfide deposit on the Mid-Atlantic Ridge. *Geology* **1996**, *24*, 1147–1150. [\[CrossRef\]](#)
64. Bau, M.; Balan, S.; Schmidt, K.; Koschinsky, A. Rare earth elements in mussel shells of the Mytilidae family as tracers for hidden and fossil high-temperature hydrothermal systems. *Earth Planet. Sci. Lett.* **2010**, *299*, 310–316. [\[CrossRef\]](#)
65. Song, X.Y.; Hou, Z.Q.; Wang, Y.L.; Zhang, C.J.; Cao, Z.M.; Li, Y.G. The mantle plume features of Emeishan basalts. *Mineral. Petrol.* **2002**, *22*, 27–32. (In Chinese with English Abstract)
66. Zhu, C.Q.; Xu, M.; Yuan, Y.S.; Zhao, Y.Q.; Shan, J.N.; He, Z.G.; Tian, Y.T.; Hu, S.B. Palaeo-geothermal response and record of the effusing of Emeishan basalts in Sichuan basin. *Chin. Sci. Bull.* **2010**, *55*, 474–482. [\[CrossRef\]](#)
67. Wang, R.H.; Tan, Q.Y.; Fu, J.Y.; Mou, C.L.; Cheng, J.X.; Wang, Z.H. The sedimentary-tectonic evolution and sedimentary response of mantle plume in Emeishan. *Earth Sci. Front.* **2011**, *18*, 201–210.
68. Taylor, K.G.; Gawthorpe, R.L.; Curtis, C.D.; Marshall, J.D.; Awwiller, D.N. Carbonate cementation in a sequence-stratigraphic framework: Upper Cretaceous sandstones, Book Cliffs, Utah-Colorado. *J. Sediment. Res.* **2000**, *70*, 360–372. [\[CrossRef\]](#)
69. Huang, S.J.; Qing, H.R.; Pei, C.R.; Hu, Z.W.; Wu, S.J.; Sun, Z.L. Strontium concentration, isotope composition and dolomitization fluids in the Feixianguan Formation of Triassic, Eastern Sichuan of China. *Acta Petrol. Sin.* **2006**, *22*, 2123–2132.
70. Yang, X.Y.; He, S.; He, Z.L.; Wang, F.R.; Li, T.Y. Characteristics and pale-fluid activity implications of fluid-inclusion and isotope of calcite veins in Jingshan area. *J. China Univ. Pet.* **2013**, *37*, 19–34.
71. Fayek, M.; Harrison, T.M.; Grove, M.; McKeegan, K.D.; Coath, C.D.; Boles, J.R. In situ stable isotopic evidence for protracted and complex carbonate cementation in a petroleum reservoir, North Coles Levee, San Joaquin Basin, California, USA. *J. Sediment. Res.* **2001**, *71*, 444–458. [\[CrossRef\]](#)

72. McArthur, J.M.; Kennedy, W.J.; Chen, M. Strontium isotope stratigraphy for Late Cretaceous time: Direct numerical calibration of the Sr isotope curve based on the US Western Interior. *Palaeogeogr. Palaeoclimatol. Palaeoecol.* **1994**, *108*, 95–119. [[CrossRef](#)]
73. Wang, Z.C.; Jiang, H.; Wang, T.S.; Lu, W.H.; Gu, Z.D.; Xu, A.N.; Yang, Y.; Xu, Z.H. Paleo-geomorphology formed during Tongwan tectonization in Sichuan Basin and its significance for hydrocarbon accumulation. *Pet. Explor. Dev.* **2014**, *41*, 305–312. [[CrossRef](#)]
74. Li, W.; Liu, J.J.; Deng, S.H.; Zhang, B.M.; Zhou, H. The nature and role of Late Sinian-Early Cambrian tectonic movement in Sichuan Basin and its adjacent areas. *Acta Pet. Sin.* **2015**, *36*, 546–556.
75. Palmer, M.R.; Edmond, J.M. The strontium isotope budget of the modern ocean. *Earth Planet. Sci. Lett.* **1989**, *92*, 11–26. [[CrossRef](#)]
76. Zhao, J.Z.; Li, X.R. Methods of geochronology of petroleum accumulation. *Xinjiang Pet. Geol.* **2002**, *23*, 257–261, (In Chinese with English Abstract).
77. Chen, H.H. Advances in geochronology of hydrocarbon accumulation. *Oil Gas Geol.* **2007**, *28*, 143–150.
78. Bourdet, J.; Pironon, J.; Levresse, G.; Tritlla, J. Petroleum type determination through homogenization temperature and vapour volume fraction measurements in fluid inclusions. *Geofluids* **2008**, *8*, 46–59. [[CrossRef](#)]
79. Larson, L.T.; Miller, J.D.; Nadeau, J.E. Two sources of error in low temperature inclusion homogenization determination, and corrections on published temperatures for the East Tennessee and Laisvall deposits. *Econ. Geol.* **1973**, *68*, 113–116. [[CrossRef](#)]
80. Guo, X.W.; Chen, J.X.; Yuan, S.Q.; He, S.; Zhao, J.X. Constraint of in-situ calcite U-Pb dating by laser ablation on geochronology of hydrocarbon accumulation in petroliferous basins: A case study of Dongying sag in the Bohai Bay Basin. *Acta Pet. Sin.* **2020**, *41*, 284–291.
81. Qiu, N.; Liu, Y.F.; Liu, W.; Jia, J.K. Quantitative reconstruction of formation paleo-pressure in sedimentary basins and case studies. *Sci. China Earth Sci.* **2020**, *63*, 808–821. [[CrossRef](#)]
82. Liu, S. Formation time and formation mechanism of the Weiyuan anticline in Sichuan Basin. *J. Chengdu Univ. Technol.* **2001**, *28*, 340–343. (In Chinese with English Abstract)
83. Xu, H.L.; Wei, G.Q.; Jia, C.Z.; Yang, W.; Zhou, T.W.; Xie, W.R.; Li, C.X.; Luo, B.W. Tectonic evolution of the Leshan-Longnvsi paleo-uplift and its control on gas accumulation in the Sinian strata, Sichuan Basin. *Pet. Explor. Dev.* **2012**, *39*, 406–416. [[CrossRef](#)]
84. Mei, Q.H.; He, D.F.; Wen, Z.; Li, Y.Q.; Li, J. Geologic structure and tectonic evolution of Leshan-Longnvsi paleo-uplift in Sichuan Basin, China. *Acta Pet. Sin.* **2014**, *35*, 11–25.
85. Liang, J.J. The difference of hydrocarbon accumulation of Sinian and Lower Palaeozoic in the middle and southwest of Sichuan Basin. *Chengdu Univ. Technol.* **2014**, 93–94.
86. Yang, Y.M.; Wen, L.; Luo, B.; Wang, W.Z.; Shan, S.J. Hydrocarbon accumulation of Sinian natural gas reservoirs Leshan-Longnvsi paleohigh, Sichuan Basin, SW China. *Pet. Explor. Dev.* **2016**, *43*, 179–188. [[CrossRef](#)]